Steel and Composite Structures, *Vol. 32, No. 1* (*2019*) *91-110*
DOI: https://doi.org/10.12989/scs.2019.32.1.091

Evaluation of ground motion scaling methods on drift demands of energy-based plastic designed steel frames under near-fault pulse-type earthquakes

Behnoud Ganjavi *, Amirali Hadinejad [a] and Amir Hossein Jafarieh [b]

Department of Civil Engineering, University of Mazandaran, Babolsar, Iran

(*Received August 9, 2018, Revised May 4, 2019, Accepted May 23, 2019*)

Abstract. In the present study, the effects of six different ground motion scaling methods on inelastic response of nonlinear steel moment frames (SMFs) are studied. The frames were designed using energy-based PBPD approach with the design concept using pre-selected target drift and yield mechanism as performance limit state. Two target spectrums are considered: maximum credible earthquake spectrum (MCE) and design response spectrum (DRS). In order to investigate the effects of ground motion scaling methods on the response of the structures, totally 3216 nonlinear models including three frames with 4, 8 and 16 stories are designed using PBPD approach and then they are subjected to ensembles of ground motions including 42 far-fault and 90 near-fault pulse-type records which were scaled using the six different scaling methods in accordance to the two aforementioned target spectrums. The distributions of maximum inter-story drift over the height of the structures are computed and compared. Finally, the efficiency and reliability of each ground motion scaling method to estimate the maximum nonlinear inter-story drift of special steel moment frames designed by energy-based PBPD approach are statistically investigated, and the most suitable scaling methods with the lowest dispersion for two groups of earthquake ground motions are introduced.

Keywords: near-fault earthquakes; pulse period; steel moment frame; scaling methods; performance-based-plastic design; seismic drift demand

1. Introduction

Nonlinear dynamic analysis of structures is being used increasingly in seismic provisions. The main challenge for engineers is how the required earthquake ground motion excitation must be scaled as it is not logical to be used directly in time history analysis. It is well known that the nonlinear response of structure is often very sensitive to the scaling of the input excitation. Therefore, during the past decades, many different methods have been proposed for scaling the ground motion excitation. Generally, the intensity or severity of an earthquake excitation is quantitatively expressed by an intensity measure (IM) such as peak ground acceleration (PGA) or spectral acceleration corresponding to the first vibration mode of the structure. As mentioned above, many studies have been performed on ground motion selection and scaling methods during the past two decades. Shome *et al*. (1998) suggested that a more effective method for estimation of nonlinear response of the structure corresponding to an earthquake magnitude (M) and distance (R) could be preliminary estimation of mean spectral acceleration before conducting nonlinear analyses. They showed that scaling a suit of ground motions based on the fundamental period of a given structure can be considered as the best method. In another study, Cordova *et al*. (2000) presented a method to determine seismic response and collapse probability of the structure for moment frame systems. They proposed an index which reflects the intensity and configuration of the spectrum, and demonstrated that their proposed index has the capability to significantly reduce the record dependency of the structural response in nonlinear time history analyses. A practical method was introduced by Naeim *et al*. (2004) through searching into thousands of records to find a desirable collection which their spectrums are compatible with the target design spectrum. This method uses genetic algorithm to find optimum ensemble of seven records and their scaling factors. In a related study, Baker and Allin Cornell (2005) considered an intensity criterion which employed spectral acceleration using the difference between spectral acceleration and mean spectral acceleration obtained from an attenuation expression. Following to this study, Baker and Allin Cornell (2006) suggested a conditional mean spectrum which derived for a magnitude and distance corresponding to the target earthquake intensity. They showed that the difference at spectral acceleration corresponding to the first mode of vibration is an important index. Luco and Bazzurro (2007) investigated the influence of the scaling on randomly selected records from a specific range of magnitude and distance, up to a level of spectral acceleration corresponding to the fundamental mode which was based on the nonlinear structural drift response of SDOF and MDOF systems. Huang *et al*. (2009) studied four methods of scaling including: (1) geometric mean scaling of pairs of earthquakes; (2) spectrum compatible with records; (3) scaling the spectral acceleration of the first

*Corresponding author, Associate Professor,
E-mail: b.ganjavi@umz.ac.ir
[a] M.S. Graduate, E-mail: a.hadinejad@umz.ac.ir
[b] Assistant Professor, E-mail: ah.jafarieh@umz.ac.ir

http://www.techno-press.org/?journal=scs&subpage=6
ISSN: 1229-9367 (Print), 1598-6233 (Online)

mode of vibration to target spectral acceleration level; and (4) scaling ground motions per the distribution of spectral demands. They concluded that for nonlinear SDOF systems, spectrum-matching scaling, underestimates the median displacement demands. A scaling method based on modal-pushover analysis (MPA) to scale ground motions for employing in nonlinear response analysis of buildings was proposed by Kalkan and Chopra (2010). In a related study, Sumer *et al*. (2009) showed that the MPA method is an improved procedure over the ASCE 7-05 (2005) method because it considers the strength characteristics of the building and the effects of higher modes. Multi-modes ground motion scaling method which considers the dominating modes in estimating structural responses was suggested by Weng *et al*. (2010). Heo *et al*. (2010) investigated the accuracy of two ground motion scaling methods including scaling spectral ordinates at the structural fundamental period and spectrum matching. It was concluded that spectrum matching could be more suitable than the common code-compliant scaling methods. In confirmation of this study, Roy *et al*. (2014) analyzed a number of single-story and multi-story symmetric and asymmetric-plan buildings to evaluate the accuracy of spectrum matching methods. They found that the time-domain spectral matching procedure can predict more accurately seismic demand parameters e.g., story drifts. This scaling method was also employed by many researchers for optimum seismic design of fixed-base and soil-structure systems (Hajirasouliha and Moghaddam 2009, Hajirasouliha and Pilakoutas 2012, Ganjavi and Hao 2013, Ganjavi *et al*. 2016, Hajirasouliha *et al*. 2016, Ganjavi and Gholamrezatabar 2018). Most of the above-mentioned studies were limited to a specific scaling method for a simple type structural model. Recently, in one of the comprehensive studies, Abedi-Nik and Khoshnoudian (2014) studied effect of different ground motion scaling methods that were already proposed by researchers on seismic demands of shear-building soil-structure systems. They concluded that a suitable scaling method cannot predict all responses with sufficient accuracy. However, their study were based on the results of shear-building structures that may not be applicable for more realistic building structures such as moments-resisting frames that are basically designed based on the “strong- column weak-beam” design philosophy.

Many researches demonstrated that structures designed based on new seismic design procedures can experience large plastic deformations during strong earthquakes. This is while, many seismic provisions are based on elastic methods which lead to inappropriate distribution of plastic deformations and shear forces in structure when subjected to moderate and severe earthquakes. In order to design structures which have desirable and predictable performance during design earthquakes, nonlinear behavior of the structure must be considered in design procedure directly, which cannot be achieved by elastic analyses. To overcome this deficiency, Leelataviwat *et al*. (1998) suggested a new plastic design method based on displacement control for steel moment frames using energy equalization concept for a preselected yield mechanism with sufficient strength and ductility. This method is a limit state design criterion based on relative target drift and preselected yield mechanism. Since the preliminary proposed design method did not consider the force reduction, displacement amplification factors and energy dissipation capacity which play important roles in seismic design, it could lead to conservative and unconservative designs for long-period and short period structures, respectively. Following to this study, Lee (2002) improved this method and proposed performance-based plastic design (PBPD) approach. They modified energy balance equation with a factor which led to larger design base shear for short period systems corresponding to constant acceleration range of design spectrum and also smaller design base shear for systems with longer periods. Then, Chao and Goel (2006) extended PBPD method to braced frames and showed that this method can effectively prevent braced frames from collapse. Goel *et al*. (2010) studied the reinforced concrete moment frames designed based on PBPD method. Results of extensive inelastic analyses showed that for the frames designed based on strong column-sway mechanisms, the story drifts and ductility demands were well within the target values. During the past ten years several studies have been conducted to apply the PBPD method in different fixed-base building structures (Banihashemi *et al*. 2015, Chan-Anan *et al*. 2016, Mortezaie and Rezaie 2018, Fakhraddini *et al*. 2018a, b). More recently, Ganjavi *et al*. (2019) investigated the effect soil-structure interaction on drift demands distribution along the height of the steel moment frame structures designed with performance-based-plastic design (PBPB) approach under 20 strong ground motions. The adequacy of different lateral loading patterns was also parametrically investigated. In addition, the influences of soil-structure interaction key parameters, fundamental period and ductility ratio on dispersion of the drift results were evaluated and discussed.

In this research for the first time, the effects of six different ground motion scaling methods on inelastic response of nonlinear steel moment resisting frames (SMRFs) designed using energy-based Performance-Based Plastic Design (PBPD) approach subjected to two suits of far-fault and near-fault pulse-type ground motions are parametrically studied. In order to investigate the effects of ground motions scaling methods on seismic response of the structures, three frames with 4, 8 and 16 stories were designed using PBPD approach and then are subjected to 42 far-field 90 near-field pulse-type records which were scaled using each of the scaling methods in accordance to two target spectrums. Then, the distributions of maximum nonlinear drift over the height of totally 3216 nonlinear SMRFs are statistically calculated. The accuracy of different ground motions scaling methods are evaluated to estimate the maximum nonlinear inter-story drift of moment frames and the most suitable and reliable approaches with the lowest dispersion are introduced for each of the earthquake ground motion ensembles.

2. Modeling and assumptions

PBPD method is based on two key factors: target displacement or drift and pre-selected yield mechanism. Employing a desirable yield mechanism and target drift that correspond to a given hazard level control the level and distribution of damage in a structure. In addition, the design base shear for a given hazard level, its distribution along the height of the structure and also plastic design are the three main elements of this sophisticated approach. The design base shear can be derived by equating the required work to push the structure monotonically up to the target displacement to the energy needed by an equivalent elastic-plastic SDOF (EP-SDOF) system to reach the same target displacement. Also, the distribution of lateral load over the height of the structure is determined based on relative story base shear in order to match the results with the responses of dynamic analyses as well. At the final stage, a preselected mechanism based on plastic analysis is utilized to determine the requirements of the designated yielding frame members to reach the pre-selected yield mechanism.

2.1 Design base shear

As mentioned above, the determination of the design base shear is one of the key factors in PBPD method. It is calculated by equating the required work to push the structure to target displacement monotonically with the energy needed for an equivalent EP-SDOF system to reach the same target displacement. For perfectly elastic-plastic behavior, the total energy can be easily computed using pseudo velocity and acceleration which can be written as

$$E_e + E_p = \gamma E = \gamma(1/2\, MS_V^2) = \frac{1}{2}\gamma M(\frac{T}{2\pi}S_a . g)^2 \qquad (1)$$

where M is the total weight of the system; E_e and E_P are respectively the elastic and plastic energy required for the structure to reach the target displacement. Also, S_v and S_a are spectral pseudo velocity and pseudo acceleration, respectively. γ is energy modification factor which can be determined as follows

$$\gamma = \frac{2\mu_s - 1}{R_\mu^2} \qquad (2)$$

In accordance to the Eq. (2), energy modification factor is dependent on ductility (μ_s) and strength reduction factor (R_μ) which could be determined from Fig. 1(a). There are several researches which investigated the relationship between R_μ and μ_s. In this study, the idealized inelastic spectra presented by Newmark-Hall (1973) for EP-SDOF is used to consider the relationship between μ_s, R_μ and fundamental period of the structure as shown in Fig. 1(b).

Using a selected yield mechanism and equating of lastic energy to the external work of lateral forces leads to

$$E_p = \sum_{i=1}^{n} F_i h_i \theta_p \qquad (3)$$

Employing the Eqs. (1)-(3), the work-energy equation can be written as

$$\frac{1}{2}\left(\frac{W}{g}\right)\times\left(\frac{T}{2\pi}\times\frac{V_y}{W}g\right)^2 + V_y\left(\sum_{i=1}^{N}\lambda_i h_i\right)\theta_p = \frac{1}{2}\gamma\left(\frac{W}{g}\right)\times\left(\frac{T}{2\pi}S_a g\right)^2 \qquad (4)$$

By solving and simplifying the Eq. (4), the base shear can be determined from Eq. (5).

$$\frac{V_y}{W} = \frac{-\alpha + \sqrt{\alpha^2 + 4\gamma S_a^2}}{2} \qquad (5)$$

where α is a dimensionless parameter and can be calculated by Eq. (6)

$$\alpha = \left(h^* \times \frac{\theta_p 8\pi^2}{T^2 g}\right) \qquad (6)$$

In Eq. (6), θ_p is plastic rotation that corresponds to the target drift and h^* is equal to $\sum_{i=1}^{N}\lambda_i h_i$.

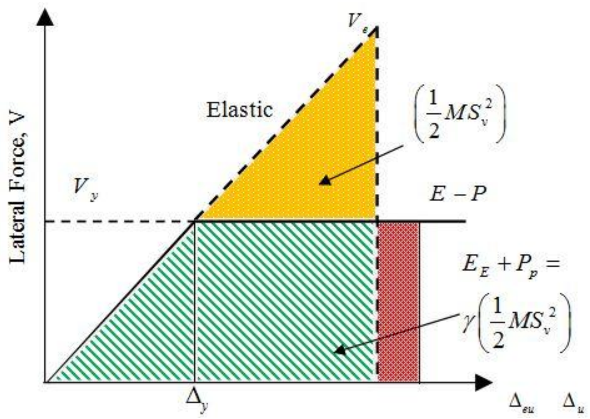

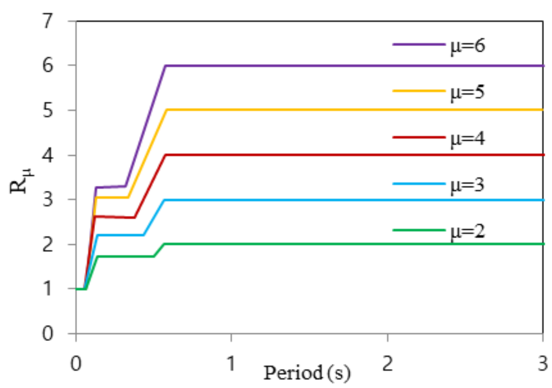

Fig. 1 (a) Idealized response of an EP-SDOF system based on energy concept; (b) inelastic response spectrum for an EP-SDOF system

2.2 Lateral force distribution

The design lateral forces can be determined by lateral force distribution factor (β_i) which has been calculated by nonlinear time history analyses for a number of structures through Eq. (7).

$$\beta_i = (\frac{V_i}{V_n})^{\alpha} == \left(\frac{\sum_{j=i}^{n} w_j h_j}{w_n h_n} \right)^{0.75T^{-0.2}} V_y \tag{7}$$

in which V_i and V_n are base shear of ith story and the last story, respectively. β_i is the coefficient of proportionality in ith story level. W and h are weight and height of the story level. V_y represents as design base shear and T is fundamental period of the structure. The lateral force in ith story level is determined from Eq. (8)

$$F_i = \left(\beta_i - \beta_{i+1}\right) V_n \tag{8}$$

2.3 Plastic design method

The preliminary goal in plastic design is to consider the elements for determining the required capacity to form the plastic hinge at the end of elements confidently. As shown in Fig. 2(a), formation of the plastic hinges at the two ends of beam and columns of the base level is the best desirable scenario for moment frame structures. For this configuration of plastic hinges (see Fig 2(b)), the equalization of external and internal work leads to

$$\sum_{i=1}^{n} 2\beta_i M_{pbr} + 2M_{pc} = \sum_{i=1}^{n} F_i h_i = \sum_{i=1}^{n} \left(\beta_i - \beta_{i+1}\right) h_i F_n \quad \text{and} \quad M_{PC} = \frac{1.1 V h_1}{4} \tag{9}$$

Where M_{pbr} is the required resisting moment at ith level and M_{pc} is the plastic moment of the first-story columns. V is total base shear and h_1 is the height of the first story and 1.1 is the over-strength to take into account for possible over-loading resulted from strain hardening phenomenon.

Having the parameter M_{pbr}, the section of beams at each level can be computed. By assuming the presumed over strength factor ξ_i at each story the beam moments considering fully strain-hardened curve is obtained. In the current study, ξ_i is assumed as 1.0 and 1.05 for the beams at top story and other stories, respectively. Based on the assumption of plastic hinge formation in columns at the top story, the value of ξ_i equal to 1.0 is adopted at that level. It should be noted that overall mechanism will not be influenced by the plastic hinges at the top story. Seismic strength values at ultimate drift level denoted by F_{iu}, can be easily estimated by Eqs. (10) and (11)

$$F_{iu} = \left(\beta_i - \beta_{i+1}\right) F_{nn} \tag{10}$$

$$\sum_{i=1}^{n} (\beta_i - \beta_{i+1}) h_i F_{nu} = M_{pc} + \sum_{i=1}^{n} \xi_i M_{pbi} \tag{11}$$

ξ_i has been already defined, and M_{pbi} = the nominal plastic moment of beam at i*th* story.

If the column is assumed as a cantilever, after updating the seismic lateral strengths, design moments of column will be computed as

$$M_c(h) = \sum_{i=1}^{n} \delta_i \xi_i M_{pbi} - \sum_{i=1}^{n} \delta_i F_{iu} (h_i - h) \tag{12}$$

in which the h column's moment at the level of h is denoted by $M_c(h)$, and δ_i is a step function taken the value as

$$\delta_i = 1 \quad if\ h \le h_i \quad and \quad \delta_i = 0 \quad if\ h > h_i \tag{13}$$

The $P_c(h)$ defined as the axial force of each column at the level of h, can be determined by Eq. (14)

$$P_c(h) = \sum_{i=1}^{n} \delta_i (2\xi_i M_{pbi} / L) + P_{cg}(h) \tag{14}$$

where L and $P_{cg}(h)$ are respectively the beams' span length and the gravity-loads axial force at the level h. Having the previously obtained values of $M_c(h)$ and $P_c(h)$, by conventional design codes the column can be designed as

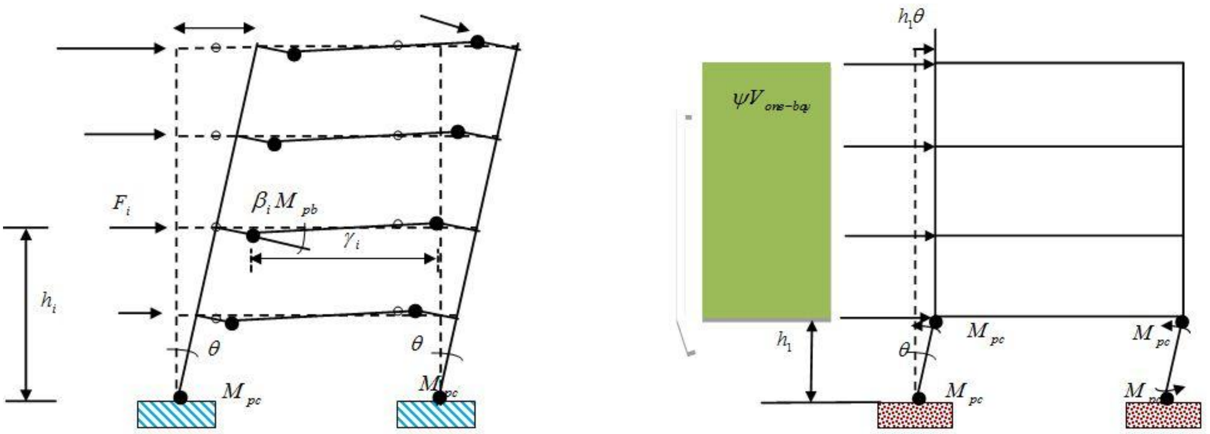

Fig. 2 (a) Single-bay frame prototype with predefined mechanism and plastic hinges in beams and columns end; (b) Frame with Soft-Story Mechanism beam-column elements.

2.4 Design of the frames and validation of nonlinear analyses

As discussed previously, three steel moment frames having 4, 8 and 16 stories respectively representing low-mid- and high-rise buildings have been designed, using PBPD procedure for parametric study. A typical story weight of 845.5 kN has been assigned to each story. The seismic loads were determined based on IBC-2015. The site location was assumed to be in Riverside–California (Latitude, Longitude: 33.982, -117.374) with S_S = 1 andS_1 = 0.6. The risk category is IV and the site class is considered C and D. Knowing the required parameters, the seismic response coefficients (C_s) for three frames were calculated and mentioned in the Table 1. Also, the section properties of the steel moment frame prototypes are shown in Fig. 3. The frames have been modeled in OpenSees software (OPENSEES 2016) using nonlinear fiber elements. The first mode periods of vibration of 4-, 8- and 16-story frames are 0.76, 1.26 and 2.14 sec, respectively. In order to study the performance of the designed frames, nonlinear static

Table 1 Design parameters of the prototypes used in this study for target inter-story drift ratio of 2%

Story No.	T(s)	C_s	Yield drift	θ_p	α	γ	Design V/W
4	0.76	0.94	0.01	0.01	2.04	0.75	0.283
8	1.26	0.66	0.01	0.01	1.38	0.75	0.207
16	2.14	0.47	0.01	0.01	0.97	0.75	0.146

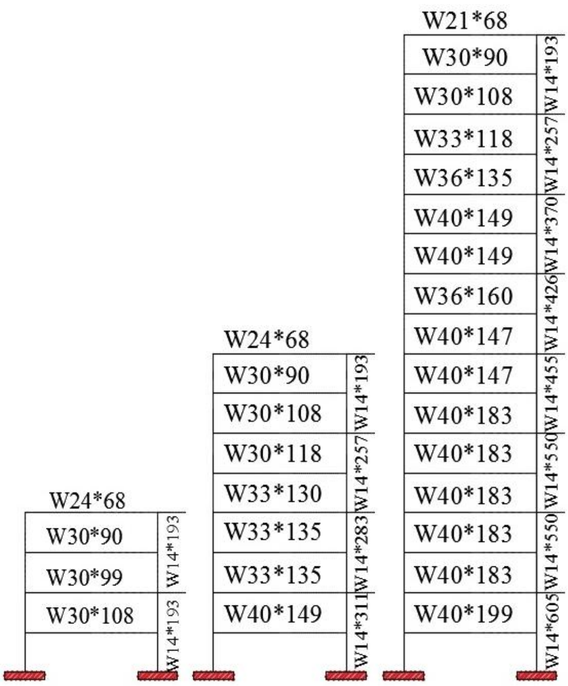

Fig. 3 Elevation and section properties of the steel moment frame prototypes designed based on PBPD for target inter-story drift ratio of 2%

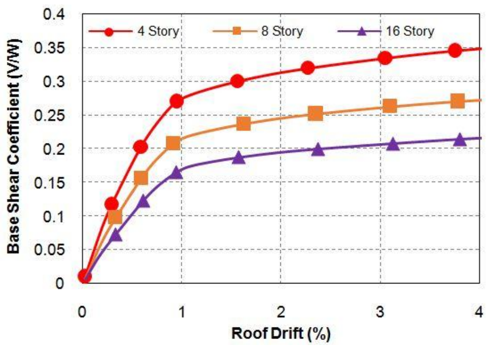

Fig. 4 Pushover curves for three frames in current study

pushover analyses were conducted. The pushover plots are shown in Fig. 4. Comparing the values of V/W and yield drift for 4-, 8- and 16-story frames, considered in design procedure and provided in Table 1, with the corresponding values that can be estimated from pushover plots shows very negligible differences. This is in good agreement with results obtained from the studies of Lee (2002).

In addition, to validated the results of this study nonlinear dynamic analyses were conducted on the 16-story frame prototype when subjected to the same earthquake ground motion of EL-Centro utilized by Lee (2002). A comparison of the results of relative distributions of maximum story shears along the height of the building for different values of β depicted in Fig. 5 shows an excellent agreement, demonstrating the accuracy of the modeling assumptions and analysis procedures of this study.

3. Scaling the ground motions

In order to compare the results of different time history analyses, the ground motions must be scaled because the responses are highly sensitive to the intensity of the excitations. Selection of an appropriate intensity measure denoted hereafter as “Scaling Method” (SM) can significantly reduce the time of analysis for computing seismic response parameters, which leads to a more reliable estimation of seismic demands of structures. The lowest dispersion in seismic response estimations can be obtained by applying an appropriate SM, so the number of required records for analysis can be reduced. In this research, six different methods of scaling are considered to evaluate the seismic performance of steel moment frames designed by PBPD approach as follows:

1) SM-1. Peak ground acceleration (PGA): Intensity of an earthquake is a function of maximum amplitude of ground motion such as acceleration and velocity. So, the ground motion can be scaled to a constant PGA.

$$SM_1 = S_a(T=0) \tag{15}$$

2) SM-2. Spectral acceleration corresponds to the first mode of vibration which has been used as seismic intensity parameter for scaling the ground motions in many investigations.

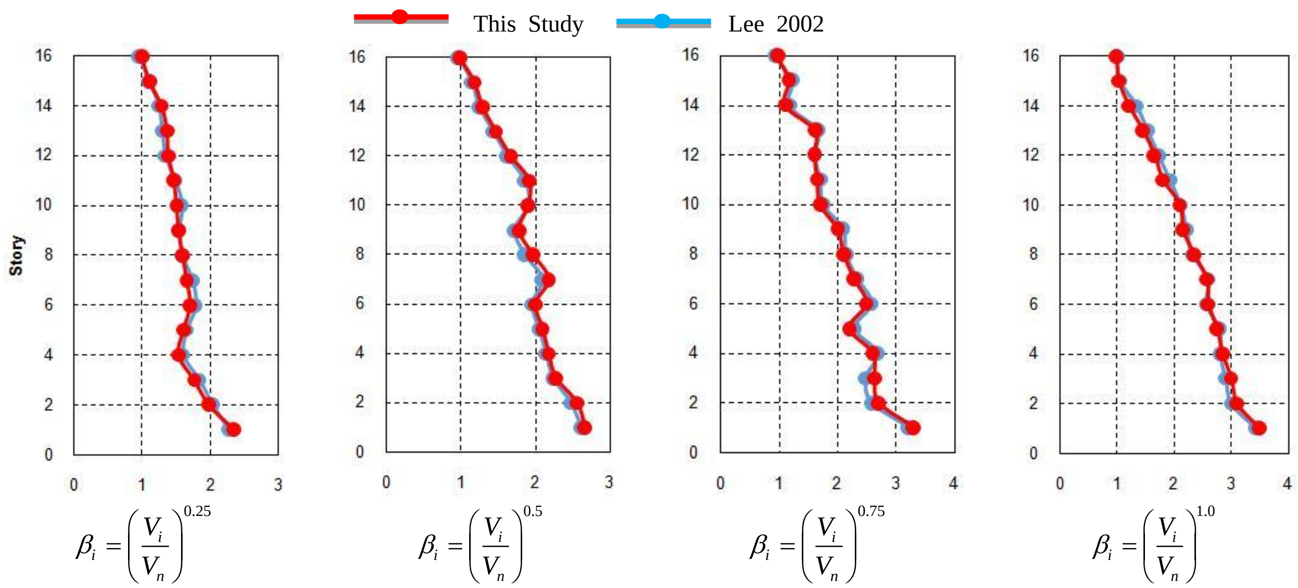

Fig. 5 Comparison of the relative distributions of maximum story shears along the height of the building for different values of β; 16-Story Frames - V_i / V_n; El Centro earthquake

$$SM_2 = S_a(T_1) \tag{16}$$

3) SM-3. Cordova intensity criterion (2000): In order to take into account the effects of period lengthening as a result of nonlinear behavior of structure, Cordova *et al*. (2000) introduced secondary intensity parameters which considers the spectral configuration. The suggested SM consists of spectral acceleration at two different structural periods.

$$SM_3 = \sqrt{S_a(T_1)S_a(2T_1)} \tag{17}$$

4) SM-4. Luco and Cornel intensity criterion (2007): This intensity criterion considers the second mode contribution and period lengthening as a result of nonlinear behavior of the structure besides the first mode of vibration.

$$SM_4 = \frac{S_d^I(T_1,\xi_1,d_y)}{S_d(T_1,\xi_1)}\sqrt{\left[PF_1^{[2]}S_d(T_1,\xi_1)\right]^2 + \left[PF_2^{[2]}S_d(T_2,\xi_2)\right]^2} \tag{18}$$

Where, $S_d^I(T_1,\xi_1,d_y)$ is inelastic spectral displacement corresponding to the first mode of structure and S_d (T_1,ξ_1) is elastic spectral acceleration that corresponds to the first mode period of vibration. $PF_j^{[k]}$ is the contribution factor of jth mode of vibration corresponding to the first k modes of structure. To avoid conducting nonlinear time history analyses for SDOF systems, the inelastic spectral acceleration can be determined by equivalent linear elastic system. In order to calculate the equivalent period and damping of the system the equations proposed by FEMA-440 (2005) can be used as follows

$$for \rightarrow 1 < \mu < 4 \begin{cases} T_{eq} = T_1\left[1 + 0.2(\mu-1)^2 - 0.038(\mu-1)^3\right] \\ \xi_{eq} = (100\xi_1 + 4.9(\mu-1)^2 - 1.1(\mu-1)^3)/100 \end{cases} \tag{19}$$

According to the equivalent damping, the design spectrum must be reduced. For this purpose FEMA-440 (2005) suggested the following expressions

$$(S_a)_\xi = (S_a)_{5\%} / B(\xi) \tag{20}$$

$$B(\xi) = 4/(5.6094 - Ln(\xi \times 100)) \tag{21}$$

5) SM-5. Three-parameter scaling method: the studies carried out by Vamvatsikos and Cornell criterion (2002) showed that using a specific spectral value like $S_a(T_1)$ is useful for the structures which their responses are influenced by only the first mode of vibration. For this type of structures, a value for period which is usually proportional to the increase in the fundamental period is considered to take into account the effects of nonlinear behavior. On the other hand, when the higher modes effects are significant, using only a single spectral value is not sufficient. Therefore, the researchers proposed an intensity criterion based on three spectral accelerations as follows

$$SM_5 = \sqrt[3]{S_a(\tau_a)S_a(\tau_b)S_a(\tau_c)} \tag{22}$$

Where τ_a, τ_b and τ_c are arbitrary periods which are considered as T_2, T_1 and $1.5T_1$, respectively.

6) SM-6. Code-based scaling method: seismic regulations provisions such as NEHRP (BSSC -2015) and ASCE 7-16 (2016) propose to scale the records in period range of $0.2T_1$ to $1.5T_1$. In this scaling method, the average of 5% damped response spectra for a suit of the selected ground motions must be greater than the corresponding ordinate of the target response spectrum in the specified period range.

Table 2 Number of near-fault ground motions for each frame

$0.35 \leq T_1/T_p \leq 3.0$			
Story	T_1	$T_1/T_p < 1$	$T_1/T_p \geq 1$
4	0.75	29	3
8	1.26	31	17
16	2.14	32	30

4. Near-fault pulse-type and far-fault ground motions selection

A large number of ground motions were used for nonlinear dynamic analyses which are classified primarily in accordance to their frequency content characteristics. Hence, ordinary far-fault and near-fault pules type ground motions are utilized and separately considered for scaling methods evaluation.

Table 3 Properties of near-fault ground motions used in this study

NO	Earthquake Name	Year	Station Name	(M_w)	R (km)	V_{S30} (m/s)	T_p (s)	PGA (g)	PGV (cm/s)
1	Imperial Valley-06	1979	Agrarias	6.5	0.7	242.05	2.34	0.3	53.3
2	Imperial Valley-06	1979	EC County Center FF	6.5	7.3	192.05	4.42	0.22	70.8
3	Imperial Valley-06	1979	El Centro - Meloland Geot. Array	6.5	0.1	264.57	3.42	0.38	116.5
4	Imperial Valley-06	1979	El Centro Array #4	6.5	7	208.91	4.79	0.37	81.1
5	Imperial Valley-06	1979	El Centro Array #5	6.5	4	205.63	4.13	0.38	96.4
6	Imperial Valley-06	1979	El Centro Array #6	6.5	1.4	203.22	3.77	0.44	121.6
7	Imperial Valley-06	1979	El Centro Array #7	6.5	0.6	210.51	4.38	0.47	111.8
8	Imperial Valley-06	1979	El Centro Differential Array	6.5	5.1	202.26	6.27	0.37	71.3
9	Imperial Valley-06	1979	Holtville Post Office	6.5	7.5	202.89	4.82	0.24	73.3
10	Irpinia, Italy-01	1980	Bagnoli Irpinio	6.9	8.2	649.67	1.71	0.19	38.1
11	Irpinia, Italy-01	1980	Sturno (STN)	6.9	10.8	382	3.27	0.32	71.0
12	Morgan Hill	1984	Coyote Lake Dam (SW Abut)	6.2	0.5	561.43	1.07	1.31	76.8
13	Morgan Hill	1984	Gilroy Array #6	6.2	9.9	663.31	1.23	0.27	37.3
14	Superstition Hills-02	1987	Parachute Test Site	6.5	0.9	348.69	2.39	0.45	143.9
15	Loma Prieta	1989	Gilroy - Historic Bldg.	6.9	11	308.55	1.64	0.27	43.6
16	Loma Prieta	1989	Gilroy Array #2	6.9	11.1	270.84	1.73	0.4	46.12
17	Loma Prieta	1989	Gilroy Array #3	6.9	12.8	349.85	2.64	0.36	44.8
18	Loma Prieta	1989	Saratoga - Aloha Ave	6.9	8.5	380.89	4.57	0.31	53.5
19	Loma Prieta	1989	Saratoga - W Valley Coll.	6.9	9.3	347.9	5.65	0.28	62.0
20	Cape Mendocino	1992	Petrolia	7	8.2	422.17	3	0.71	96.6
21	Northridge-01	1994	Jensen Filter Plant	6.7	5.4	373.07	3.16	0.38	101.41
22	Northridge-01	1994	Jensen Filter Plant Generator	6.7	5.4	525.79	3.54	0.51	66.0
23	Northridge-01	1994	LA - Sepulveda VA Hospital	6.7	8.4	380.06	0.93	0.75	77.5
24	Northridge-01	1994	LA Dam	6.7	5.9	628.99	1.62	0.47	86.3
25	Northridge-01	1994	Newhall - Fire Sta	6.7	5.9	269.14	1.37	0.7	115.5
26	Northridge-01	1994	Newhall-W Pico Canyon Rd.	6.7	5.5	285.93	2.98	0.41	118.3
27	Northridge-01	1994	Pacoima Kagel Canyon	6.7	7.3	508.08	0.73	0.53	56.2
28	Northridge-01	1994	Rinaldi Receiving Sta	6.7	6.5	282.25	1.25	0.88	148.9
29	Northridge-01	1994	Sylmar-Converter Sta	6.7	5.3	251.24	2.98	0.64	106.1
30	Northridge-01	1994	Sylmar-Converter Sta East	6.7	5.2	370.52	3.53	0.84	113.8
31	Northridge-01	1994	Sylmar-Olive View Med FF	6.7	5.3	440.54	2.44	0.8	130.1
32	Kobe, Japan	1995	KJMA	6.9	1	312	1.09	0.86	105.3
33	Kobe, Japan	1995	Port Island (0 m)	6.9	3.3	198	2.83	0.43	102.9
34	Kobe, Japan	1995	Takarazuka	6.9	0.3	312	1.81	0.66	95.5
35	Kobe, Japan	1995	Takatori	6.9	1.5	256	1.55	0.75	153.3
36	Kocaeli, Turkey	1999	Yarimca	7.5	4.8	297	4.95	0.28	90.6
37	Chi-Chi,Taiwan	1999	CHY006	7.6	9.8	438.19	2.57	0.32	58.3
38	Chi-Chi,Taiwan	1999	CHY024	7.6	9.6	427.73	6.65	0.28	61.5
39	Chi-Chi,Taiwan	1999	CHY101	7.6	9.9	258.89	5.34	0.39	108.9

Table 3 Continued

NO	Earthquake Name	Year	Station Name	(M_w)	R (km)	V_{S30} (m/s)	T_p (s)	PGA (g)	PGV (cm/s)
40	Chi-Chi,Taiwan	1999	TCU036	7.6	19.8	478.07	5.38	0.13	63.2
41	Chi-Chi,Taiwan	1999	TCU039	7.6	19.9	540.66	9.33	0.2	58.1
42	Chi-Chi,Taiwan	1999	TCU046	7.6	16.7	465.55	8.04	0.14	31.3
43	Chi-Chi,Taiwan	1999	TCU049	7.6	3.8	487.27	10.22	0.3	56.4
44	Chi-Chi,Taiwan	1999	TCU051	7.6	7.6	350.06	10.38	0.17	52.7
45	Chi-Chi,Taiwan	1999	TCU052	7.6	0.7	579.1	11.96	0.51	209.1
46	Chi-Chi,Taiwan	1999	TCU053	7.6	6	454.55	13.12	0.22	37.1
47	Chi-Chi,Taiwan	1999	TCU056	7.6	10.5	403.2	8.94	0.17	45.3
48	Chi-Chi,Taiwan	1999	TCU059	7.6	17.1	272.67	7.78	0.13	64.1
49	Chi-Chi,Taiwan	1999	TCU063	7.6	9.8	476.14	6.55	0.17	79
50	Chi-Chi,Taiwan	1999	TCU065	7.6	0.6	305.85	5.74	0.81	136.7
51	Chi-Chi,Taiwan	1999	TCU068	7.6	0.3	487.34	12.29	0.47	342.2
52	Chi-Chi,Taiwan	1999	TCU075	7.6	0.9	573.02	5	0.31	105.0
53	Chi-Chi,Taiwan	1999	TCU076	7.6	2.7	614.98	4.73	0.42	71.3
54	Chi-Chi,Taiwan	1999	TCU082	7.6	5.2	472.81	8.1	0.21	56.2
55	Chi-Chi,Taiwan	1999	TCU087	7.6	7	538.69	10.4	0.12	45.4
56	Chi-Chi,Taiwan	1999	TCU101	7.6	2.1	389.41	10.32	0.18	76.7
57	Chi-Chi,Taiwan	1999	TCU102	7.6	1.5	714.27	9.63	0.3	104.9
58	Chi-Chi,Taiwan	1999	TCU103	7.6	6.1	494.1	8.69	0.13	67.1
59	Chi-Chi,Taiwan	1999	TCU128	7.6	13.1	599.64	9.02	0.13	60.6
60	Chi-Chi,Taiwan	1999	TCU136	7.6	8.3	462.1	8.88	0.14	61.6
61	Duzce, Turkey	1999	Bolu	7.1	12	293.57	0.88	0.82	65.7
62	Denali, Alaska	2002	TAPS Pump Station#10	7.9	2.7	329.4	3.16	0.33	121.5
63	Chi-Chi, Taiwan-04	1999	CHY074	6.2	6.2	553.43	2.44	0.35	44.0
64	Chi-Chi, Taiwan-06	1999	TCU078	6.3	11.5	443.04	4.15	0.26	38.4
65	Chi-Chi, Taiwan-06	1999	TCU080	6.3	10.2	489.32	1.02	0.49	39.2
66	Cape Mendocino	1992	Bunker Hill FAA	7	12.2	566.42	5.36	0.22	43.6
67	Cape Mendocino	1992	Centerville Beach, Naval Fac	7	18.3	459.04	1.97	0.47	26.3
68	Bam, Iran	2003	Bam	6.6	1.7	487.4	2.02	0.81	124.2
69	Parkfield-02, CA	2004	PARKFIELD - EADES	6	2.9	383.9	1.22	0.45	35.8
70	Parkfield-02, CA	2004	Slack Canyon	6	3	648.09	0.85	0.35	53.2
71	Parkfield-02, CA	2004	Parkfield-Cholame 1E	6	3	326.64	1.33	0.48	51.7
72	Parkfield-02, CA	2004	Parkfield-Cholame 3W	6	3.6	230.57	1.02	0.55	43.4
73	Parkfield-02, CA	2004	Parkfield-Cholame 4W	6	4.2	410.4	0.7	0.58	38.3
74	Parkfield-02, CA	2004	Parkfield - Fault Zone 9	6	2.9	372.26	1.13	0.16	27.0
75	Parkfield-02, CA	2004	Parkfield - Fault Zone 12	6	2.6	265.21	1.19	0.38	56.6
76	Parkfield-02, CA	2004	PARKFIELD - STONE CORRAL 1E	6	3.8	260.63	0.57	0.85	43.3
77	Niigata, Japan	2004	NIGH11	6.6	8.9	375	1.8	0.54	65.5
78	Montenegro, Yugo.	1979	Bar-Skupstina Opstine	7.1	7	462.23	1.44	0.4	62.56
79	Montenegro, Yugo.	1979	Ulcinj - Hotel Olimpic	7.1	5.8	318.74	1.97	0.24	62.8
80	L'Aquila, Italy	2009	L'Aquila - V. Aterno - Centro Valle	6.3	6.3	475	1.07	0.5	42.1
81	L'Aquila, Italy	2009	L'Aquila - V. Aterno -F. Aterno	6.3	6.5	552	1.18	0.41	31.6
82	L'Aquila, Italy	2009	L'Aquila - Parking	6.3	5.4	717	1.98	0.39	46.2
83	Chuetsu-oki	2007	Joetsu Kakizakiku Kakizaki	6.8	11.9	383.43	1.4	0.46	91.0
84	Darfield, New Zealand	2010	DSLC	7	8.5	295.74	7.83	0.24	65.8
85	Darfield, New Zealand	2010	GDLC	7	1.2	344.02	6.23	0.72	128.7

Table 3 Continued

NO	Earthquake Name	Year	Station Name	(M_w)	R (km)	V_{S30} (m/s)	T_p (s)	PGA (g)	PGV (cm/s)
86	Darfield, New Zealand	2010	HORC	7	7.3	326.01	9.92	0.46	106.1
87	Darfield, New Zealand	2010	LINC	7	7.1	263.2	7.37	0.45	116.4
88	Darfield, New Zealand	2010	ROLC	7	1.5	295.74	7.14	0.39	85.7
89	Darfield, New Zealand	2010	TPLC	7	6.1	249.28	8.93	0.27	74.1
90	El Mayor-Cucapah	2010	Westside Elementary School	7.2	11.4	242	7.08	0.24	60.7

Table 4 Properties of ordinary far-fault ground motions used in this study

NO	Earthquake Name	Year	Station Name	(M_w)	R (km)	V_{S30} (m/s)	PGA (g)	PGV (cm/s)
1,2	Northern Calif-03	1954	Ferndale City Hall	6.5	27.02	219.31	0.16,0.2	36.05,26.2
3,4	San Fernando	1971	LA - Hollywood Stor FF	6.61	22.77	316.46	0.22,0.19	21.71,16.93
5,6	Imperial Valley-06	1979	Delta	6.53	22.03	242.05	0.24,0.35	26.31,32.98
7,8	Imperial Valley-06	1975	El Centro Array #12	6.53	17.94	196.88	0.14,0.12	21.48,22.98
9,10	Victoria, Mexico	1980	Chihuahua	6.33	18.96	242.05	0.15,0.1	26.18,48
11,12	Coalinga-01	1983	Cantua Creek School	6.36	24.02	274.73	0.23,0.29	26.15,26.24
13,14	Coalinga-01	1983	Parkfield - Fault Zone 7	6.36	31.21	297.46	0.12,0.12	21.36,14.77
15,16	Chalfant Valley-02	1986	Bishop - LADWP South St	6.19	17.17	303.47	0.25,0.18	19.62,19.53
17,18	Superstition Hills-02	1987	El Centro Imp. Co. Cent	6.54	18.2	192.05	0.36,0.26	48.05,41.77
19,20	Superstition Hills-02	1987	Westmorland Fire Sta	6.54	13.03	193.67	0.17,0.21	23.5,32.32
21,22	Loma Prieta	1989	Agnews State Hospital	6.93	24.57	239.69	0.17,0.16	33.5,18.65
23,24	Loma Prieta	1989	Hollister - South & Pine	6.93	27.93	282.14	0.37,0.18	62.97,30.89
25,26	Loma Prieta	1989	Hollister City Hall	6.93	27.6	198.77	0.25,0.22	38.88,45.49
27,28	Loma Prieta	1989	Hollister Differential Array	6.93	24.82	215.54	0.27,0.28	44.22,35.79
29,30	Loma Prieta	1989	Palo Alto - 1900 Embarc.	6.93	30.81	209.87	0.21,0.2	41.62,21,64
31,32	Kobe, Japan	1995	Abeno	6.9	24.85	256	0.22,0.23	21,24,24.76
33,34	Kobe, Japan	1995	Fukushima	6.9	17.85	256	0.18,0.22	31.39,30.75
35,36	Kobe, Japan	1995	Morigawachi	6.9	24.78	256	0.21,0.13	27.03,23,7
37,38	Kobe, Japan	1995	OSAJ	6.9	21.35	256	0.08,0.07	19.23,15.12
39,40	Kobe, Japan	1995	Yae	6.9	27.77	256	0.16,0.15	21.18,21.72
41,42	Chi-Chi, Taiwan-03	1999	CHY036	6.2	36.4	233.14	0.08,0.1	19.56,15.57

4.1 Near-fault pulse-type ground motions

The pulse period of near-fault ground motions is an important parameter in studying the inelastic response of the multistory building systems. Because the near-fault ground motions have distinctly different frequency contents with pulse-type characteristics, they are separately classified based on the ratio of pulse period of ground motions to a fundamental period of structures to evaluate the seismic responses of multistory buildings (Park 2007). Many previous studies showed that near-fault earthquakes can have significant effect on seismic response of structures (Alavi and Krawinkler 2000, Park 2007, Ghowsi and Sahoo 2015, Beiraghi 2018). For structures which are designed based on seismic regulations, pulse like earthquakes may lead to substantial non-uniform distribution of inter-story drift demand over the height of the structure. In order to investigate the response of systems to near-fault ground motions, the records are selected in accordance with the ratio of the fundamental period of the structure to the pulse period of a given ground motion velocity. In this regard, Alavi and Krawinkler (2000) found that the behavior of multistory frames is strongly dependent on the fundamental period of the system in comparison to the period of the pulse. For instance, if the ratio of fundamental period of the system to the pulse period is less than 1 ($T_1 < T_p < 1$), irrespective of the strength of the structure, the maximum ductility demand takes place in lower level of the building while for $T_1/T_p < 1$, the larger ductility demand is expected in top stories. In this research, the near fault records were selected based on the studies of Baker *et al*. (2011). Therefore, a large number of 90 near-fault pulse-type records with forward directivity which cover an extensive range of pulse period were selected. The ground motions have been recorded on site classes C and D based on IBC-2015 (2015). The moment magnitude of the selected earthquakes is between 6 and 7.9, and the closest distance of the fault rupture to the site is less than 20 km. The maximum velocity of the ground (PGV) is greater than 20 cm/s. The classification of the records corresponding to the period range of $0.35 \leq T_1/T_p \leq 3.0$ is used in this investigation, which is in accordance to the research conducted by Park (2007) for SMF structures. It should be noted that all near-fault records are rotated with MATLAB software (2014) 90 degrees in direction of the fault rupture and the components perpendicular to the fault are utilized in this research. The main characteristics of the near-fault records along with their pulse periods are provided in Table 2. The structures which were designed based on PBPD approach are subjected to the near-fault records, and the analyses were divided into two groups with $T_1/T_p \geq 1$ and $T_1/T_p < 1$. Considering the period of the structure, the number of records for each group is determined as shown in Table 3. Since for the 4-story building, the number of near fault records is only three with $T_1/T_p \geq 1$, so all records are considered together for this frame prototype.

4.2 Ordinary far-fault ground motions

The second suit of the earthquake excitation are the ground motions recorded on more than about 13 km from the fault rupture zone without pulse-type characteristics, which are denoted here as ordinary far-fault ground motions. The 42 far-fault ground motions which have no predominant pulse correspond to the earthquakes with distance to rupture region between 13 km and 40 km, i.e., $13 \leq R \leq 40$. The magnitudes of earthquakes events vary from 6 to 7 ($6 \leq M_w \leq 7$) with PGV greater than 20 cm/s. All ground motions are recorded on site class D based on IBC-2015 and NEHRP recommendation provision (BSSC 2015).

For each event, both of horizontal components were considered for the nonlinear dynamic analyses. The main characteristics of the far-fault records are provided in Table 4.

5. Target spectrum

In order to utilize each ground motion scaling method for conducting nonlinear dynamic time history analyses, one of the most required parameters is the spectral acceleration that corresponds to some periods of interest which should be determined from target spectrum.

Usually, design response spectrum (DRS), maximum credible earthquake (MCE) spectrum and also the spectrum resulted from attenuation relationships for a specific earthquake are used as target spectra. Since the smoothed spectra could not be assigned to a specific earthquake, as they are envelope of a number of response spectrums, utilization of them can lead to conservative results. In this research the MCE spectrum was taken from USGS website (2018) for Riverside-California region. The spectra corresponding to hazard levels of 2% and 10% probability of occurrence in 50 years were considered as MCE spectrum and design response spectrum (DRS), respectively, which are both illustrated in Fig. 6. It should be noted that the reason for considering MCE spectrum is that near-fault ground motions generally tend to control the 2/50 hazard level in relatively high seismic region, which is defined as that corresponding to 2 percent probability of exceedance of a given ground motion intensity measure in 50 years.

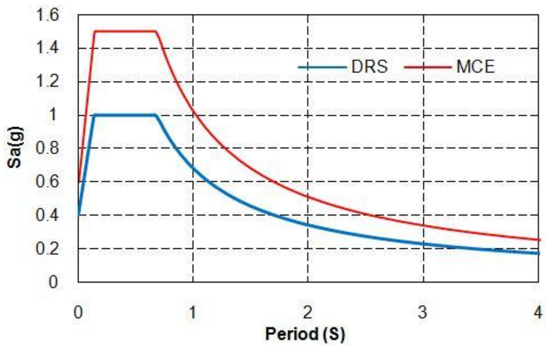

Fig. 6 DRS and MCE target spectra used for scaling ground motions

6. Studying the median and mean values of maximum drifts for different scaling methods

Utilizing a scaling method (SM) for scaling a suit of ground motions requires specifying the correlation between a given scaling criterion and the design purpose for conducting time history analysis. In other words, a SM criterion can be more suitable for a specific structural response such as drift and ductility demands than the others like force and moment demands. In this section, the results of the mean values of maximum drifts for three frames with fundamental period of 0.76, 1.26 and 2.14 s were studied under 42 far-fault and 90 near-fault records using the six aforementioned scaling methods. To this end, two types of averaging criterion including the arithmetic mean (or simply mean) and geometric *mean* (or simply median) are considered to compare the results obtained from different scaling methods. The first one, i.e., *mean*, is defined as the sum of the sampled values divided by the number of items Eq. (23); and the second one, i.e., *median*, is defined here as the exponential of the average of the natural logarithm of the values of the data points as defined by Eq. (24). The median is an appropriate representation of the central tendency of data which is lognormally distributed and reduces the amount of skewing due to outliers in the data points (Park 2007). Nevertheless, if enough samples are not present to evaluate distribution types (e.g., lognormal or normal), because of the data points, the mean values can give a reasonable representation of the central tendency.

$$Mean\ (IDR_m) = \sum_{i=1}^{n} (IDR_m)_i \Big/ n \tag{23}$$

$$Median\ (IDR_m) = e^{\left(\frac{1}{n}\sum_{i=1}^{n} Ln((IDR_m)_i)\right)} \tag{24}$$

In Eqs. (23) and (24), n is the number of records and $(IDR_m)_i$ is the maximum drift of the structure subjected to ith record. The efficiency of the different SMs are investigated for both hazard levels of MCE and DRS separately. The mean values of maximum drifts along the data points corresponding to all ground motions for three frames using various ground motions scaling methods at MCE hazard level are shown in Figs. 7-9. In these figures,

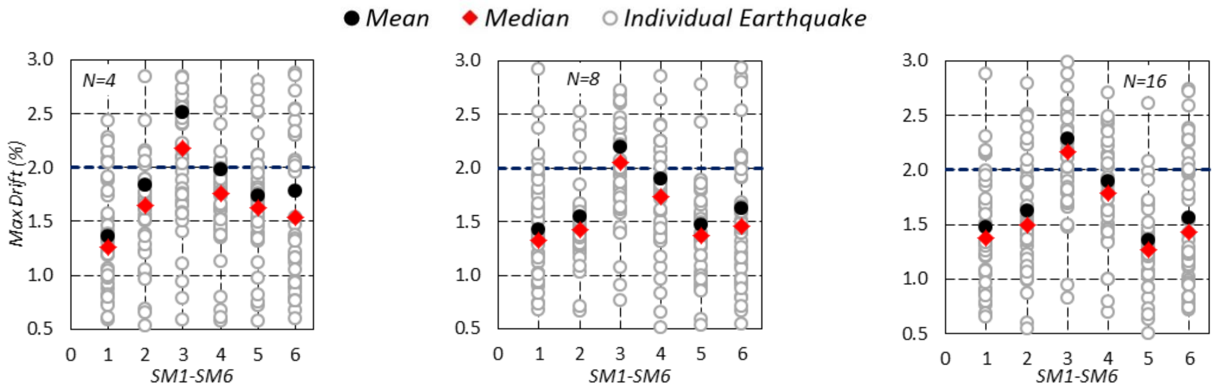

Fig. 7 Comparison of mean (or median) maximum drifts under far-fault earthquakes for different SMs (DRS hazard level)

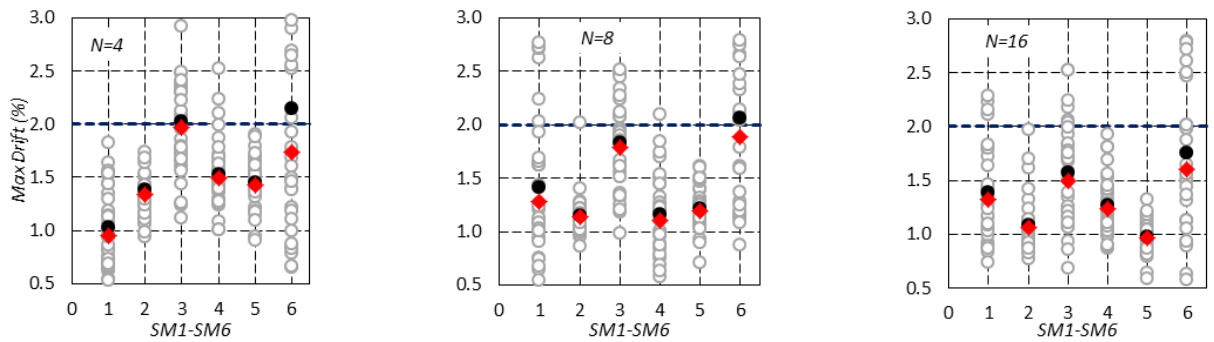

Fig. 8 Comparison of mean (or median) maximum drifts under near-fault earthquakes with $T_1/T_p < 1$ for different SMs (DRS hazard level)

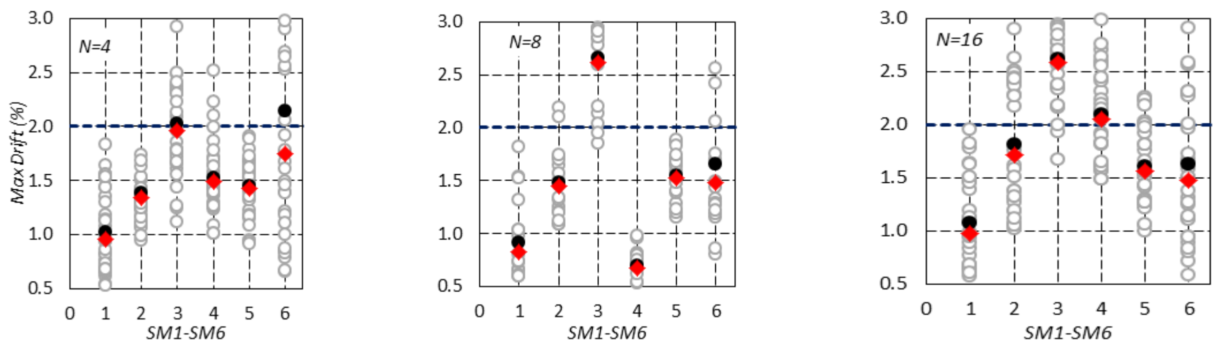

Fig. 9 Comparison of mean (or median) maximum drifts under near-fault earthquakes with $T_1/T_p \geq 1$ for different SMs (DRS hazard level)

the horizontal dashed line belongs to the target design drift for comparison. However, it should be noted that for 2/50 MCE hazard level the design drift ratio is 3%, which needs to be taken as a realistic value for comparison. In fact, the reason for considering the MCE hazard level is to examine that whether the DRS based designed structures are in average safe when they are to be subjected to an ensemble of ground motions with higher intensity?

Figs. 7-9 show the results for mean and median values of maximum drift using 6 scaling methods corresponding to only for SM-3 method the mean value of maximum drift is above the line of target drift. The values estimated by all other SMs are lower than the target drift for DRS hazard level. The same results can approximately be observed for DRS hazard level. From Fig. 7, it can be concluded that near-fault records as well. However, the mean and median values of the SM-3, in almost all cases, are still over the target line, which are more pronounced for the mid- and high-rise buildings subjected to the suit of near-fault ground motions with $T_1/T_p \geq 1$. Moreover, it is demonstrated that depending on the ground motions classification, i.e., far-fault and pulse-type near-fault records, each scaling method affects the dispersion of the results in different manners such that it might be difficult to find the most appropriate SM for all structural models. Therefore, it is mandatory to investigate this phenomenon in more details which will be done in the next sections.

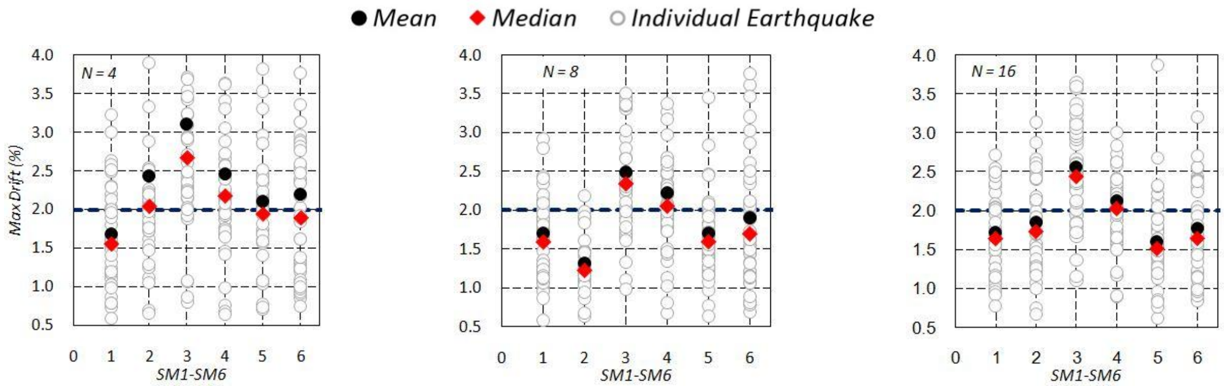

Fig. 10 Comparison of mean (or median) maximum drifts under far-fault earthquakes for different SMs (MCE hazard level)

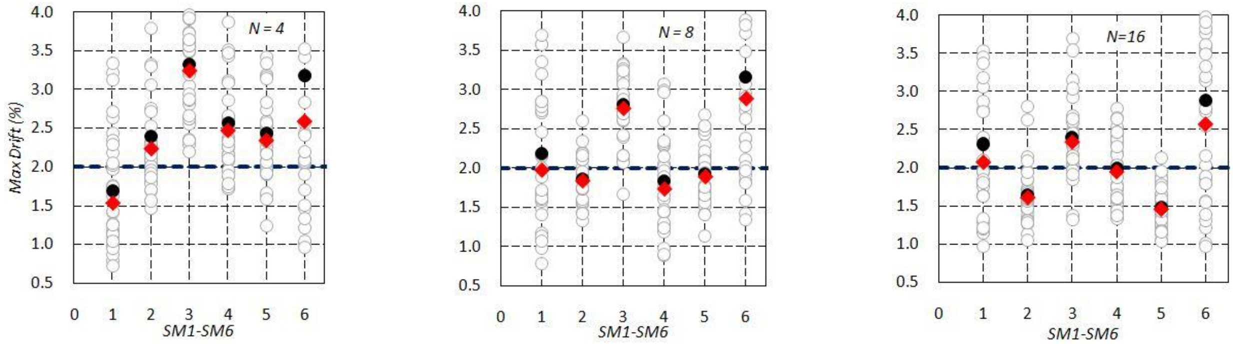

Fig. 11 Comparison of mean (or median) maximum drifts under near-fault earthquakes with $T_1/T_p < 1$ for different SMs (MCE hazard level)

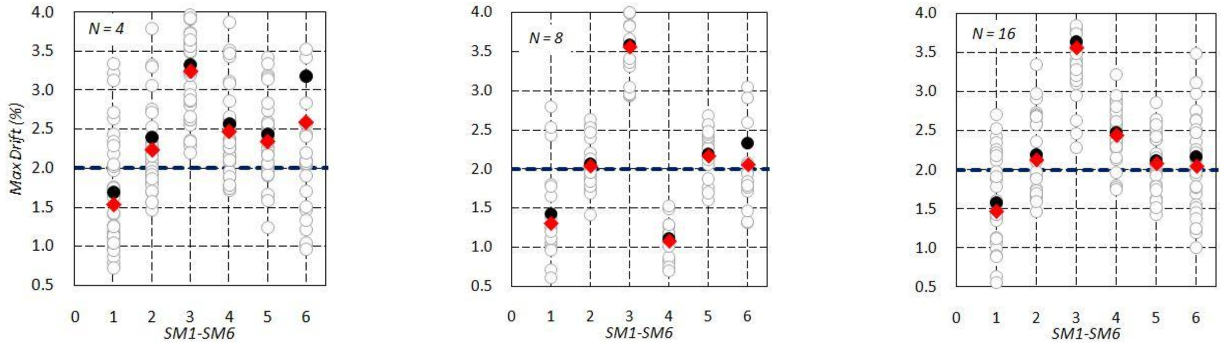

Fig. 12 Comparison of mean (or median) maximum drifts under near-fault earthquakes with $T_1/T_p \geq 1$ for different SMs (MCE hazard level)

Figs. 10-12 show the results for mean and median values of maximum drift using 6 scaling methods corresponding to MCE hazard level. Because the results for DRS spectrum correspond to lower intensities in comparison with MCE level, it is clear that the mean values for MCE level are greater than their corresponding values for DRS level. Similar to the DRS hazard level, as shown in Fig. 10, while structures were subjected to the far-fault records, the differences between median and mean of the maximum drifts when compared to the target drift are not significant. It can be observed that when the number of stories increases the differences become smaller. This can be attributed to the lower ductility demand for structures with longer periods. According to the period of the 4-story frame, the response is mostly influenced by the constant acceleration region of the spectrum in which the structural response is very sensitive to the variation of acceleration in short-period range; hence, the difference between the mean and target drift increases. For the case of 16-story frame, although SM-3 have the capability to consider the effect of nonlinear behavior of the structure, the differences between mean IDR_m and the target values are significant when compared to other scaling methods. It seems that $2T_1$, which has been taken into account for SM-3, cannot be a good representative for considering nonlinear behavior of the structure especially for the systems with higher periods.

The results for the structures subjected to near-fault records with $T_1/T_p < 1$ are depicted in Fig. 11. As can be seen, except for the SM-1, the mean and median of the drifts for the 4-story frame are always larger than the target drift and similar to the results of far-fault records, the difference between mean and target drifts decreases by increasing the number of stories.

Fig. 12 shows the results for near-fault records with $T_1/T_p \geq 1$. As can be observed, the mean values of the maximum drift of the structures are mostly larger than the target drifts and the difference is more pronounced when compared to the two previous cases illustrated in Figs. 10 and 11, implying that the ratio of pulse period of ground motions to a fundamental period of structures significantly affects the response of the structures. However, considering the fact that the target drift corresponding to 2/50 MCE hazard level in relatively high seismic region is about 3%, one may conclude that the designed structures based on 10/50 DRS hazard level, in average, can be safe when subjected to a suit of ground motions that were scaled based on 2/50 MCE hazard level. For the case with $T_1/T_p \geq 1$, the highest value belongs to the SM-3 in all frames. This will be more discussed in the upcoming sections. Among the scaling methods, for short-period structure, i.e., 4-story frame, the mean values determined by SM-1, which is based on PGA, are smaller than those of the other SMs for all ground motions groups.

7. Assessment of maximum drift distribution over height of the structures using different scaling cethods

In this section, the effect of scaling methods on height-wise distribution of maximum drift demands for three groups of earthquake ground motions with two hazard levels of DRS and MCE are investigated. To better compare the results, the mean values of drift demands are computed and the results for each family of ground motions are shown separately in Figs. 13-18.

7.1 Maximum drift distribution patterns for far-fault earthquake excitations

The mean drift patterns over the height of the building prototypes under far-fault ground motions are provided in Figs. 13-14 for respectively DRS and MCE hazard levels. It is observed that, regardless of the scaling method, general drift distribution patterns for 4- and 8-story frames representing respectively low- and mid-rise building structures are almost identical for both hazard levels such that the maximum values take place in the middle stories. In DRS hazard level, except for SM-6 corresponding to the 4-story frame, the mean values for all SMs are less than the target value which is specified by vertical dashed line;

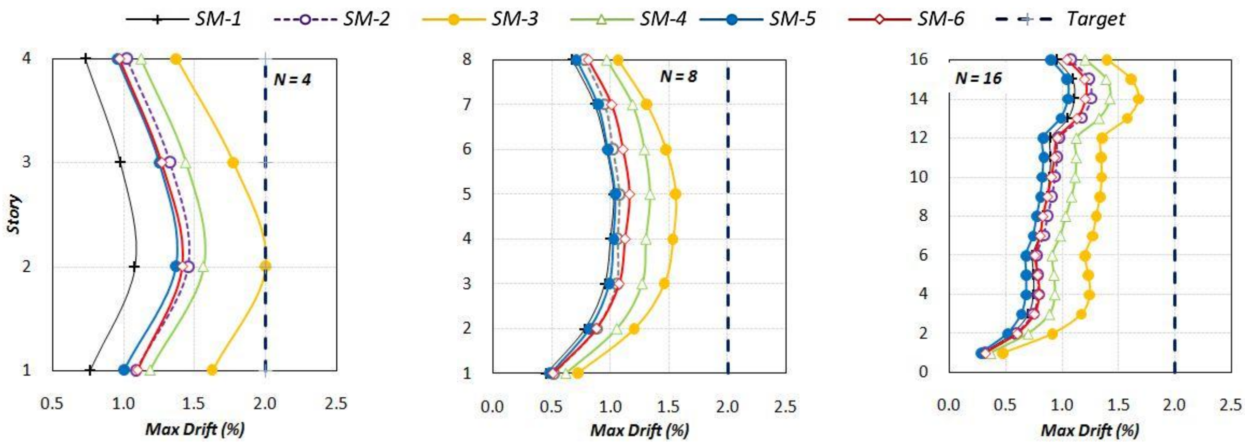

Fig. 13 Distribution of mean drifts over the height of structures subjected to far-fault earthquakes corresponding to different SMs (DRS hazard level)

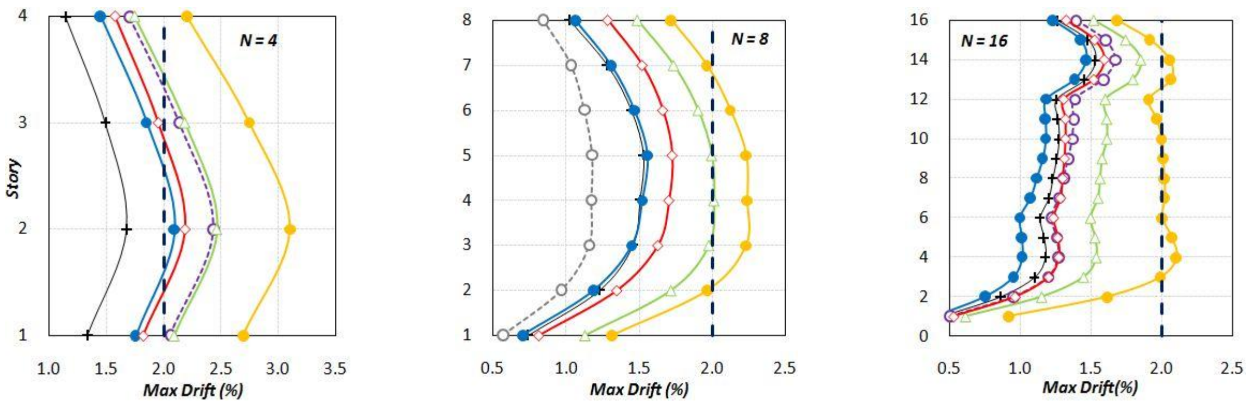

Fig. 14 Distribution of mean drifts over the height of structures subjected to far-fault earthquakes corresponding to different SMs (MCE hazard level)

however, as seen in the previous section, the drifts for some ground motions can be remarkably larger than the target one. It is also obvious that by increasing the hazard level the effect of scaling methods on the discrepancy of the results will intensify. In this case, the SM-3 has the highest value compare to the other SMs. Moreover, for the 4-story frame subjected to far-fault ground motion with MCE hazard level, with exception of SM-1, the designed models analyzed under all other SMs have the maximum drifts larger than the target one; however, the maximum drifts are still lower than the target value of 3% which is considered for 2/50 MCE hazard level. For the 16-story frame, it can be seen that by increasing the number of stories the drift distribution patterns are different for both hazard levels as well as all scaling methods such that the maximum values occur in upper stories, here in the 14th story, which can be attributed to the effect of higher modes which is more pronounced for high-rise buildings. Nevertheless, this phenomenon for SM-3 corresponding to the MCE hazard level is somewhat different and takes place in the 4th and 13th stories. It is also interesting to point out that by increasing the number of stories, i.e., 16-story model, the height-wise distribution of drift demands becomes more uniform when compared to the low- and mid-rise frames. This implies that in long-period structures designed by PBPD methods under far-fault ground motions, the dissipation of seismic energy in each structural element increases and the material capacity is more exploited.

7.2 Maximum drift distribution patterns for near-fault earthquake excitations with $T_1/T_p \geq 1$

Similar to the far-fault ground motions, the mean drift patterns over the height of the building prototypes under near-fault ground motions with $T_1/T_p \geq 1$ scaled with six different methods are plotted in Figs. 15 and 16 for respectively DRS and MCE hazard levels. As seen, the height-wise distribution of mean drift demands in the structures are somewhat different from those in buildings under far-fault records. As an instance, for the 4-story frame the maximum values corresponding to all SMs occur in the top stories. In addition, unlike to the far-fault excitation, even in lower level of hazard level of DRS, for all framed prototypes with 4, 8 and 16 stories the mean maximum drifts for SM-3 exceeded the specified target drift, which is more pronounced in low-rise frame. It was also found that the dispersion of the results corresponding to the different scaling methods is higher than far-fault earthquake records. Another difference is referred to the 16-story frame under MCE records in which the maximum drift takes place in

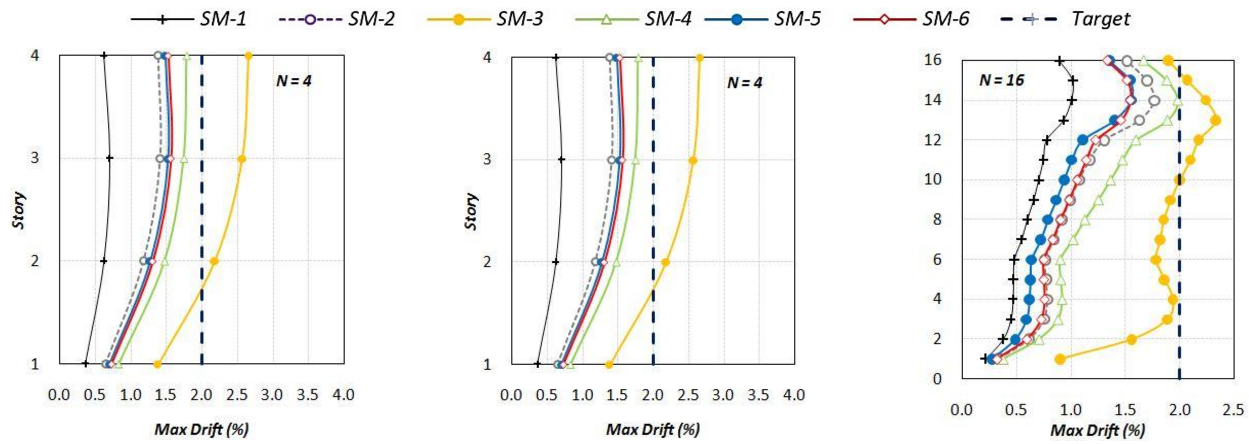

Fig. 15 Distribution of mean drifts over the height of structures subjected to near-fault earthquakes with $T_1/T_p \geq 1$ corresponding to different SMs (DRS hazard level)

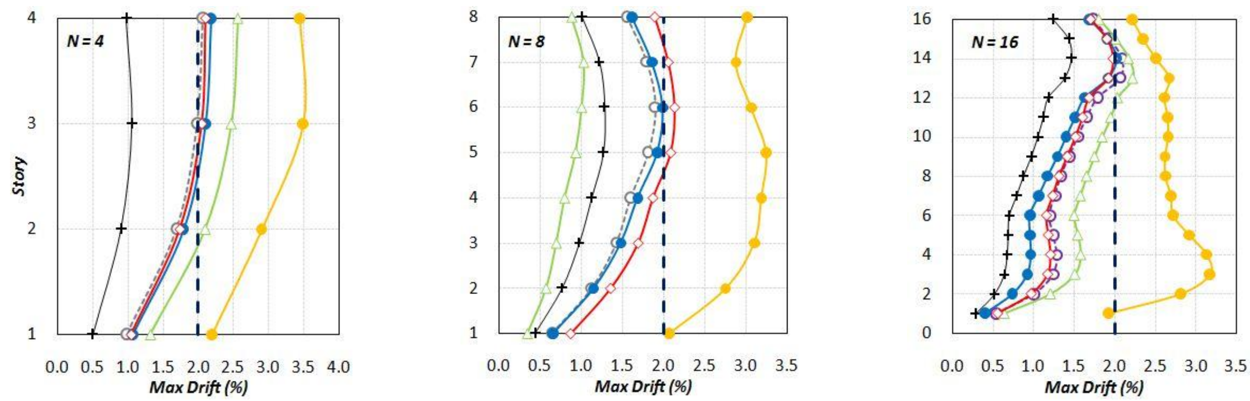

Fig. 16 Distribution of mean drifts over the height of structures subjected to near-fault earthquakes with $T_1/T_p \geq 1$ corresponding to different SMs (MCE hazard level)

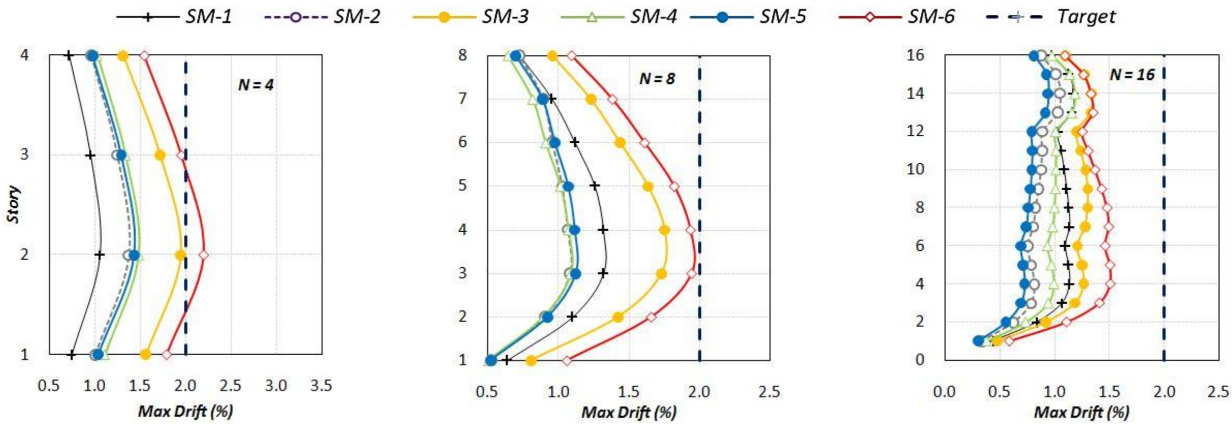

Fig. 17 Distribution of mean drifts over the height of structures subjected to near-fault earthquakes with $T_1/T_p < 1$ corresponding to different SMs (DRS hazard level)

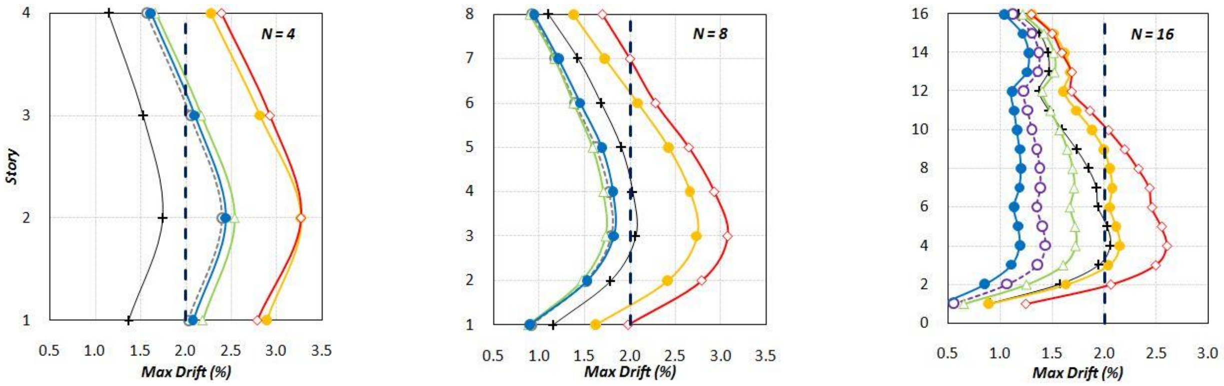

Fig. 18 Distribution of mean drifts over the height of structures subjected to near-fault earthquakes with $T_1/T_p < 1$ corresponding to different SMs (MCE hazard level)d

third story while it occurred in the fourth and thirteenth stories simultaneously for the case of far-fault earthquakes.

7.3 Maximum drift distribution patterns for near-fault earthquake excitations with $T_1/T_p < 1$

The results in this subsection are provided for the mean drift patterns over the height of the building prototypes under near-fault ground motions with $T_1/T_p < 1$ scaled with six different methods as shown in Figs. 17 and 18. A comparison between the results of these suits of earthquake records and the two families of previously discussed excitations shows that the effect of the scaling methods on the structures analyzed under records with $T_1/T_p < 1$ is significantly different from those analyzed under the two other groups. One of the main diversities is that for the case of DRS hazard level, only the maximum drift of the 4-story building model corresponding to the code-based scaling method, SM-6, exceeds from the target drift while for other models and SMs, the maximum drifts are less than the target drift. Another difference is that, opposed to the far-fault and near fault with $T_1/T_p \geq 1$, for the cases of 8- and 16-story models the maximum drifts take place in the lower stories of 3 and 4, respectively. Note that, irrespective of the frame models and the hazard levels, in general, the maximum drifts belong to the code-based scaling method of SM-6, whereas they belonged to the SM-3 for the two other ground motions groups. Overall, from the results of three ensembles of earthquake records, it is concluded that the influence of scaling methods on the maximum distribution patterns over the height of the structures designed by PBPD approach can be more sensitive to the earthquake ground motion characteristics and frequency contents rather than seismic hazard levels. Besides, in near-fault ground motion records the results are completely dependent on the ratio of the fundamental period of the structure to the pulse period of a given ground motion velocity. It is also observed that as the hazard level increases the drift distribution patterns become more non-uniform.

8. Effect of ground motion frequency contents on maximum drift for different scaling methods

To more examine the influence of frequency content of all suits of ground motions on mean of maximum drift demands resulted from different scaling methods, Fig. 19 is provided for MCE hazard level. Results obtained from short-period 4-story frame indicate that the frequency contents of ground motion ensembles do not have significant effect on the mean maximum drift demands. The only exception is for SM-6 in which the maximum drifts of

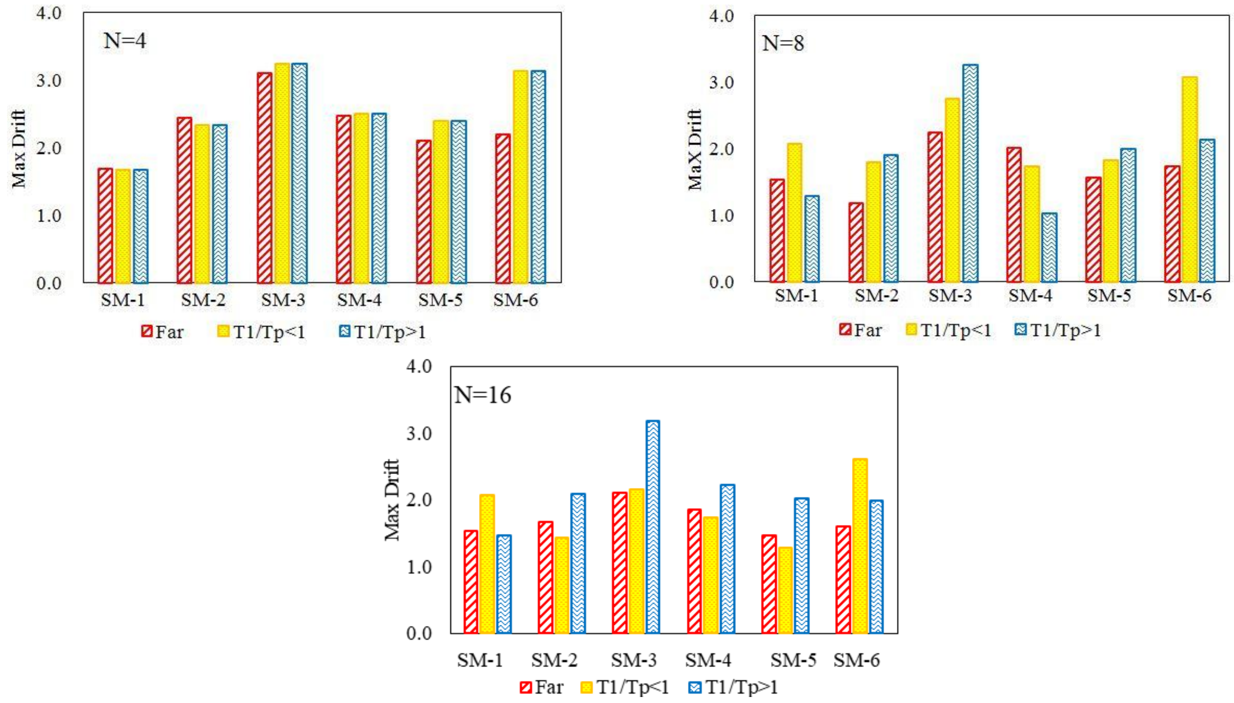

Fig. 19 Mean of maximum drift demands for structures designed by PBPD approaches scaled by different scaling methods (MCE hazard level)

the structure subjected to near-fault records are in average 43% greater than that under far-fault records. On the other hand, the impact of scaling methods on drift demands is again obvious that can increase up to two times when compared to the lowest value, which can be observable for SM-3 and SM-6. When the number of stories increases, i.e., 8-and 16-story frames, the effect of input motions and also scaling methods increase compared to the low-rise 4-story frame. It is seen that in most of the SMs, the structures that were subjected to near-fault pulse-type ground motions experienced larger drift demands with respect to those under the far-fault ground motions. The notable point is that in high-rise 16-story model subjected to the near-fault records with $T_1/T_p \geq 1$, the results of scaling methods such as SM-3, SM-4 and SM-5 in which the influence of higher modes were considered have the highest responses when compared to other SMs. To better show the role of near-fault ground motions on maximum drift demands corresponding to all scaling methods, the ratios of the mean maximum drift of each of the structural models in near-fault ground motions to that in far-fault records are computed. The results indicate that, while no significant increase for the low-rise model is observed, the ratios are considerable for the 8-and 16-story models corresponding to the different scaling methods. The highest ratios belong to SM-6 and SM-2 indicating that the mean maximum drifts of the 8-story structure subjected to near-fault records are in average respectively 78% and 61% larger than those under far-fault records. The increases are respectively 61% and 52% for the 16-story frame model, which signifies that near-fault pulse-type ground motions can have considerable effects on the seismic demands of the structures designed by PBPD approach.

9. Evaluation of dispersion of the results for different scaling methods

In order to compare the discrepancy of the results of the maximum drifts determined by different scaling methods, the dispersion of the results was calculated using the coefficient of variation of drift demands COV (IDR_m) defined as

$$COV(IDR_m)\% = (\frac{STD}{\mu_{(IDR_m)}})*100 \tag{25}$$

Where STD is standard deviation and $\mu_{(IDRm)}$ is the average of the maximum drifts of a structure subjected to an ensemble of earthquake ground motions.

9.1 Effect of seismic hazard level

In Fig. 20 the effects of seismic hazard levels on dispersion of the results for all of the frame prototypes and scaling methods subjected to 3 groups of earthquake ground motions are shown. As can be seen, except for two special cases including the SM-2 corresponding to the 4-story frame subjected to far-fault earthquakes and SM-1 corresponding to the 16-story frame subjected to near-fault earthquakes with $T_1/T_p < 1$, in all other cases the seismic hazard level has an insignificant impact on the dispersion of the results for maximum drift demands. Nevertheless, considerable influence of scaling methods for the structures subjected to the two families of near-fault records can be seen. Therefore, in subsequent sections, to more examine the dispersion of the maximum drifts only the results for MCE hazard level showing the higher seismic intensity will be discussed in detail.

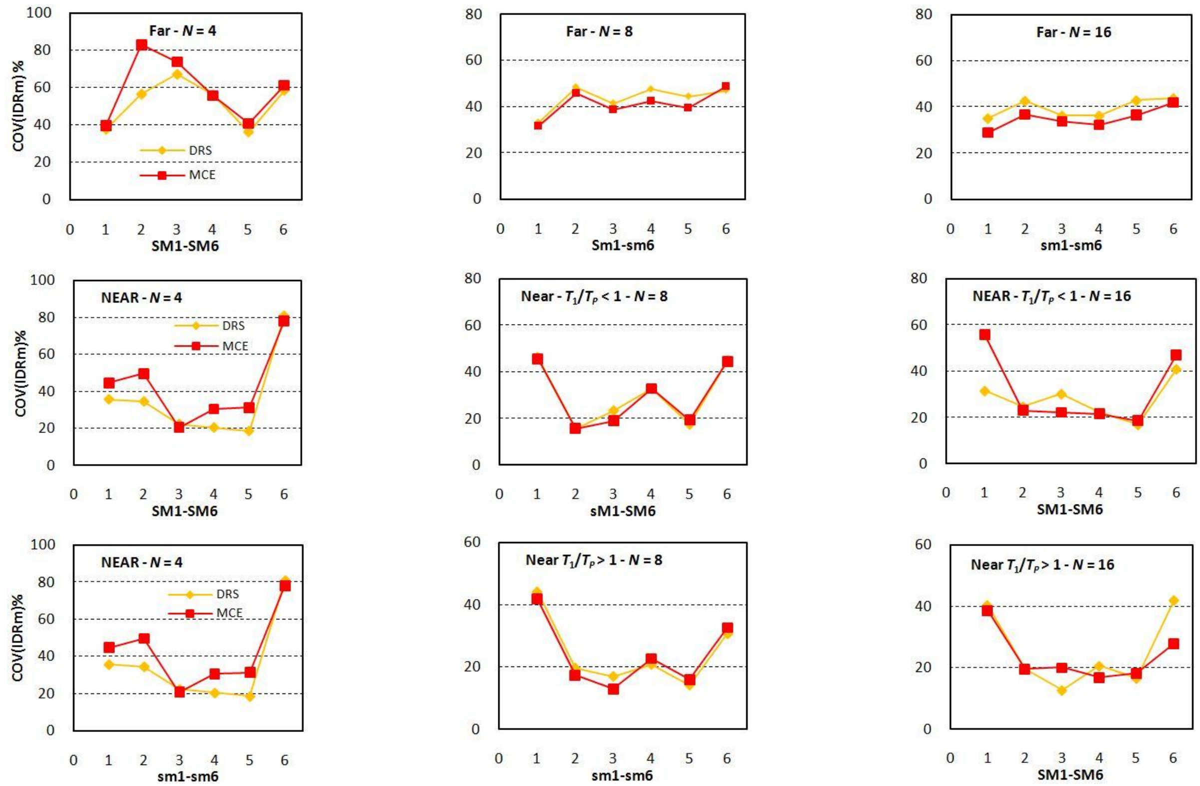

Fig. 20 Effect of seismic hazard level on the dispersion of the maximum drift demands

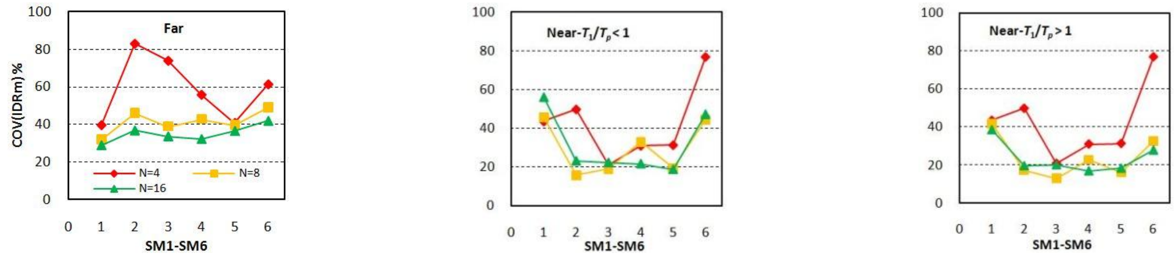

Fig. 21 Effect of number of stories on the dispersion of the maximum drift demands

9.2 Effect of number of stories

To more precisely investigate the effect of the number of stories, or fundamental period of vibration, on the dispersion of the maximum drift demands, the (COV (IDR_m)) values for the six scaling methods subjected to the three suits of earthquake ground motions are depicted in Fig. 21. It can be observed that by increasing the number of stories the COV values are generally tend to be decreased, which are more pronounced for the far-fault ground motions and near-fault records with $T_1/T_p \geq 1$, respectively. It is also shown that for mid- and high-rise buildings subjected to the far-fault records, the variations of COV (IDR_m) in different scaling methods are not large and can be practically considered negligible, whereas they are very sensitive to the scaling methods for the short-period low-rise building. In this case, the SM-2 and SM-1 have the most and the least values of COV (IDR_m). This phenomenon is less intensified for 8- and 16 story buildings subjected to the far-fault ground motions. On the other hand, in contrary to the far-fault records under which the SM-1 had the least dispersion, under near-fault ground motions SM-1 and SM-6, i.e., code-based scaling method, have the most dispersion among others. Hence, one may conclude that these two scaling methods are not appropriate for near-fault pulse-type ground motions as the results may not be reliable. On the contrary, the scaling methods of SM-3, SM-4 and SM-5 due to having the structural higher modes effect can have far better results in terms of discrepancy and reliability.

9.3 Effect of ground motion frequency content

Fig. 22 more specifically shows the effect of ground motion frequency content on the dispersion of the maximum drift demands. As observed, except for SM-1 and SM-6, the COVs of drift demands of all structural models under far-fault ground motions are much greater than those under near-fault records for other scaling methods. However, it is more intensified for the short-period low-rise building. In addition, for the structure subjected to near

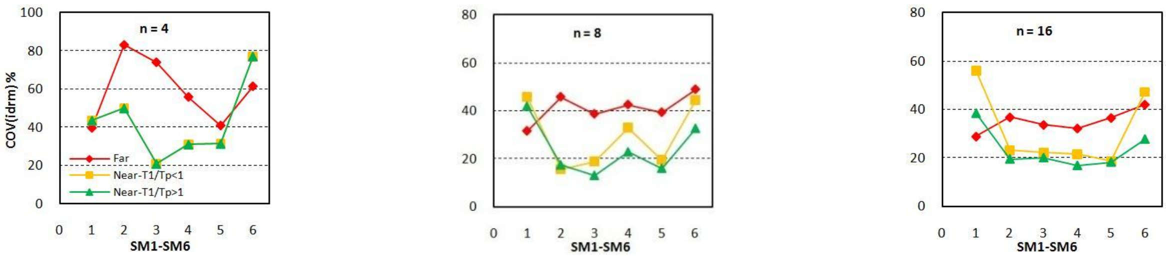

Fig. 22 Effect of the ground motion frequency content on the dispersion of the maximum drift demands

fault records, no significant variation can be seen for the SM-2 to SM-5. As a concluding remark, it can be said that for the structure subjected to an ensemble of far-fault ground motions, in average, the scaling methods of SM-1, scaled to PGA, and SM-5, proposed by Vamvatsikos and Cornell criterion (2002), can be considered as the best scaling method with the lowest dispersion.

However, for near-fault pulse-type ground motions the SM-1 will lead to very unreliable results. In this case, the scaling methods such as SM-3 and SM-5 can have more reliable results with lower dispersion compared to other SMs. Hence, in general, considering the repetition and commonality of the SM-5 in all groups of ground motion utilized in this study, this scaling method proposed by Vamvatsikos and Cornell (2002) in which the effects of higher modes and nonlinear behavior on structural periods are taken into account can be introduced as the most reliable scaling method for nonlinear dynamic analysis of the structures designed by PBPD approach.

10. Conclusions

In this research, the effects of six different ground motion scaling methods on inelastic response of nonlinear SMRFs designed using energy-based plastic design approach subjected to two suits of far-fault and near-fault pulse-type ground motions were studied. In order to investigate the effects of ground motions scaling methods on seismic response of the structures, three frames with 4, 8 and 16 stories were designed in accordance to design response spectrum (DRS) and were subjected to the ground motions scaled by different scaling methods. The results obtained from the present study can be summarized as follows:

(1) For the structures under far-fault earthquakes by increasing the number of stories, the height-wise distribution of drift demands becomes more uniform when compared to the low- and mid-rise frames. This implies that in long-period structures designed by PBPD methods under far-fault ground motions, the dissipation of seismic energy in each structural element increases and the material capacity is more exploited. However, for the case of near-fault ground motion, it was observed that as the hazard level increases the drift distribution patterns become more non-uniform. It was also seen that the mean maximum drifts of the frames are, in average, well within the corresponding target values for most of the SMs.

(2) The influence of scaling methods on the maximum drift distribution patterns can be more sensitive to the earthquake ground motion characteristics and frequency contents rather than seismic hazard levels. Besides, in near-fault ground motion records the results are completely dependent on the ratio of the fundamental period of the structure to the pulse period of a given ground motion velocity.

(3) Results obtained from the short-period 4-story frame indicate that the frequency contents of ground motion ensembles do not have significant effect on the mean maximum drift demands. The only exception is for SM-6 in which the maximum drifts of the structure subjected to near-fault records are in average 43% greater than that under far-fault records. When the number of stories increases, i.e., 8-and 16-story frames, the effect of input motions and also scaling methods increase compared to the low-rise 4-story frame. It is seen that in most of the SMs, the structures that were subjected to near-fault pulse-type ground motions experienced larger drift demands with respect to those under the far-fault ground motions. In these cases the maximum ratios are 1.78 and 1.61 for respectively the 8-and 16-story frames.

(4) The seismic hazard level has an insignificant impact on the dispersion of the results for maximum drift demands. Nevertheless, consider-able influence of scaling methods for the structures subjected to the two families of near-fault records can be seen.

(5) In contrast to the far-fault records under which the SM-1 had the lowest dispersion, under near-fault ground motions SM-1 and code-based scaling method of SM-6 have the most dispersion among others. Hence, one may conclude that these two scaling methods are not appropriate for near-fault pulse-type ground motions as the results may not be reliable. On the contrary, the scaling methods of SM-3, SM-4 and SM-5 due to having the structural higher modes effect can have far better results in terms of discrepancy and reliability.

(6) Assessment of the COVs for maximum drift demands showed that for the structure subjected to an ensemble of far-fault ground motions, in average, the scaling methods of SM-1, scaled to PGA, and SM-5, can be considered as the best scaling method with the lowest dispersion. However, for near-fault pulse-type ground motions the SM-1 will lead to

very unreliable results. In this case, the scaling methods such as SM-3 and SM-5 can have more reliable results with lower dispersion compared to other scaling methods.

(7) Overall, SM-5 scaling method proposed by Vamvatsikos and Cornell (2002) in which the effects of higher modes and nonlinear behavior on structural periods have been taken into account can be introduced as the most reliable scaling method for nonlinear dynamic analysis of the structures designed by PBPD approach. As demonstrated in this study, the dispersion of this method was low in average for all cases and its accuracy is less dependent on the hazard level, number of stories and frequency content of ground motions in comparison with the other SMs.

References

Abedi-Nik, F. and Khoshnoudian, F. (2014), "Evaluation of ground motion scaling methods in soil–structure interaction analysis", *Struct. Des. Tall Special Build.*, **23**(1), 54-66. https://doi.org/10.1002/tal.1021

Alavi, B. and Krawinkler, H. (2000), "Consideration of near-fault ground motion effects in seismic design", *Proceedings of the 12th World Conference on Earthquake Engineering*, p. 8.

ASCE/SEI 7-05 (2005), Minimum Design Loads for Buildings and Other Structures; American Society of Civil Engineers, VA, USA. https:// doi.org/10.1061/9780784408094

ASCE/SEI 7-10 (2016), Minimum Design Loads for Buildings and Other Structures; American Society of Civil Engineers, VA, USA. https:// doi.org/10.1016/j.engstruct.2015.10.048

Baker, J.W. and Allin Cornell, C. (2005), "A vector-valued ground motion intensity measure consisting of spectral acceleration and epsilon", *Earthq. Eng. Struct. Dyn.*, **34**(10), 1193-1217. https://doi.org/10.1002/eqe.474

Baker, J.W. and Allin Cornell, C. (2006), "Spectral shape, epsilon and record selection", *Earthq. Eng. Struct. Dyn.*, **35**(9), 1077-1095. https://doi.org/10.1002/eqe.571

Baker, J.W., Lin, T., Shahi, S.K. and Jayaram, N. (2011), New ground motion selection procedures and selected motions for the PEER transportation research program; Report No. 3, Pacific Earthquake Engineering Research Center, University of California, Berkeley, CA, USA.

Banihashemi, M.R., Mirzagoltabar, A.R. and Tavakoli, H.R. (2015), "Development of the performance based plastic design for steel moment resistant frame", *Int. J. Steel Struct.*, **15**(1), 51-62. https://doi.org/10.1007/s13296-015-3004-6

Beiraghi, H. (2018), "Energy demands in reinforced concrete wall piers coupled by buckling restrained braces subjected to near-fault earthquake", *Steel Compos. Struct., Int. J.*, **27**(6), 703-716. https://doi.org/ 10.12989/scs.2018.27.6.703

Building Seismic Safety Council (BSSC) (2015), NEHRP Recommended Seismic Provisions for New Buildings and Other Structures; Volume 1: Part 1 Provisions, Part 2 Commentary, FEMA P-1050-1, Washington, D.C., USA, 555. https://doi.org/10.1002/tal.1278

Chan-Anan, W., Leelataviwat, S. and Goel, S. C. (2016), "Performance-based plastic design method for tall hybrid coupled walls", *Struct. Des. Tall Special Build.*, *25*(14), 681-699. _https://doi.org/10.1002/tal.1278

Chao, S.H. and Goel, S.C. (2006), "Performance-based seismic design of eccentrically braced frames using target drift and yield mechanism as performance criteria", *Eng. J.-Am. Inst. Steel Constr. Inc.*, **43**(3), 173-200. https://doi.org/10.12989/eas.2017.13.5.443

Cordova, P.P., Deierlein, G.G., Mehanny, S.S. and Cornell, C.A. (2000), "Development of a Two-Parameter Seismic Intensity Measure and Probabilistic Assessment Procedure", In: *The second US-Japan workshop on performance-based earthquake engineering methodology for reinforced concrete building structures*, pp. 187-206.

Fakhraddini, A., Fadaee, M.J. and Saffari, H. (2018a), "A lateral load pattern based on energy evaluation for eccentrically braced frames", *Steel Compos. Struct., Int. J.*, **27**(5), 623-632. https://doi.org/10.12989/scs.2018.27.5.623

Fakhraddini, A., Saffari, H. and Fadaee, M.J. (2018b), "A hybrid force/displacement seismic design method for steel eccentrically braced frames", *Asian J. Civil Eng.*, **19**(1), 93-102. https://doi.org/10.1007/s42107-018-0010-y

FEMA-440 (2005), Improvement of nonlinear static seismic analysis procedures; Redwood City, CA, USA.

Ganjavi, B. and Gholamrezatabar, A. (2018), "More adequate seismic design force pattern for yielding structures considering structural and ground motion uncertainties effects", *Struct. Des. Tall Special Build.*; e1537. https://doi.org/10.1002/tal.1537

Ganjavi, B. and Hao, H. (2013), "Optimum lateral load pattern for seismic design of elastic shear-buildings incorporating soil–structure interaction effects", *Earthq. Eng. Struct. Dyn.*, **42**(6), 913-933. https://doi.org/10.1002/eqe.2252

Ganjavi, B., Hajirasouliha, I. and Bolourchi, A. (2016), "Optimum lateral load distribution for seismic design of nonlinear shear-buildings considering soil-structure interaction", *Soil Dyn. Earthq. Eng.*, **88**, 356-368. https://doi.org/10.1016/j.soildyn.2016.07.003

Ganjavi, B., Gholamrezatabar, A. and Hajirasouliha, I. (2019), "Effects of Soil-Structure Interaction and Lateral Design Load Pattern on Performance-Based Plastic Design of Steel Moment Resisting Frames", *Struct. Des. Tall Special Build.*, 24(1). [In Press] https://doi.org/10.1002/tal.1624

Ghowsi, A.F. and Sahoo, D.R. (2015), "Fragility assessment of buckling-restrained braced frames under near-field earthquakes", *Steel Compos. Struct., Int. J.*, **19**(1), 173-190. https://doi.org/10.12989/scs.2015.19.1.173

Goel, S.C., Liao, W.C., Reza Bayat, M. and Chao, S.H. (2010), "Performance-based plastic design (PBPD) method for earthquake-resistant structures: an overview", *Struct. Des. Tall Special Build.*, **19**(1-2), 115-137. https://doi.org/ 10.1051/matecconf/201925805014

Hajirasouliha, I. and Moghaddam, H. (2009), "New lateral force distribution for seismic design of structures", *J. Struct. Eng.*, **135**(8), 906-915. https://doi.org/10.1061/(ASCE)0733-9445(2009)135:8(906)

Hajirasouliha, I. and Pilakoutas, K. (2012), "General seismic load distribution for optimum performance-based design of shear-buildings", *J. Earthq. Eng.*, **16**(4) 443-462. https://doi.org/10.1080/13632469.2012.654897

Hajirasouliha, I., Pilakoutas, K., Reza K. and Mohammadi, R.K (2016), "Effects of uncertainties on seismic behaviour of optimum designed braced steel frames", *Steel Compos. Struct., Int. J.*, **20**(2), 317-335. https://doi.org/10.12989/scs.2016.20.2.317

Heo, Y., Kunnath, S.K. and Abrahamson, N. (2010), "Amplitude-scaled versus spectrum-matched ground motions for seismic performance assessment", *J. Struct. Eng.*, **137**(3), 278-288. https://doi.org/10.1061/(ASCE)ST.1943-541X.0000340

Huang, Y.N., Whittaker, A.S., Luco, N. and Hamburger, R.O. (2009), "Scaling earthquake ground motions for performance-based assessment of buildings", *J. Struct. Eng.*, **137**(3), 311-321. https://doi.org/10.1139/cjce-2012-0339

International Building Code (IBC) (2015), Country Club Hills, IL,

USA, International Code Council, Inc.
Kalkan, E. and Chopra, A.K. (2010), “Practical guidelines to select and scale earthquake records for nonlinear response history analysis of structures”, Report No. 1068; US geological survey open-file report, 126.
Lee, S.S. (2002), “Performance-based design of steel moment frames using target drift and yield mechanism”, Ph.D. Dissertation; University of Michigan, MI, USA.
Leelataviwat, S., Goel, S.C. and Stojadinovic, B. (1998), “Drift And Yield Mechanism Based Seismic Design And Upgrading Of Steel Moment Frames”, *Univ of Michigan*, **98**(29).
Luco, N. and Bazzurro, P. (2007), “Does amplitude scaling of ground motion records result in biased nonlinear structural drift responses?”, *Earthq. Eng. Struct. Dyn.*, **36**(13), 1813-1835. https://doi.org/10.1002/eqe.695
Luco, N. and Cornell, C.A. (2007), “Structure-specific scalar intensity measures for near-source and ordinary earthquake ground motions”, *Earthq. Spectra*, **23**(2), 357-392. https://doi.org/10.1193/1.2723158
MATLAB (2014), The Math Works, Inc., Natick, Massachusetts, United States.
Mortezaie, H. and Rezaie, F. (2018), “Effect of soil in controlling the seismic response of three-dimensional PBPD high-rise concrete structures”, *Struct. Eng. Mech., Int. J.*, **66**(2), 217-227. https://doi.org/10.12989/sem.2018.66.2.217
Naeim, F., Alimoradi, A. and Pezeshk, S. (2004), “Selection and Scaling Of Ground Motion Time Histories for Structural Design Using Genetic Algorithms”, *Earthq. Spectra*, **20**(2), 413-426. https://doi.org/10.1193/1.1719028
Newmark, N.M. and Hall, W.J. (1973), “Seismic Design Criteria for Nuclear Reactor Facilities”, Report No. 46, Building Practices for Disaster Mitigation, National Bureau of Standards, U.S. Department of Commerce, pp. 209-236.
OPENSEES (2016), OpenSees command language manual, Open system for earthquake engineering simulation. http://opensees.berkeley.edu/
Park, K. (2007), “Lateral load patterns for the conceptual seismic design of moment-resisting frame structures”, Ph.D. Dissertation; University of Maryland, MD, USA.
Roy, R., Thakur, P. and Chakroborty, S. (2014), “Scaling of ground motions and its implications to plan-asymmetric structures”, *Soil Dyn. Earthq. Eng.*, **57**, 46-67. https://doi.org/10.1016/j.soildyn.2013.11.003
Shome, N., Cornell, C.A., Bazzurro, P. and Carballo, J.E. (1998), “Earthquakes, records, and nonlinear responses”, *Earthq. Spectra*, **14**(3), 469-500. https://doi.org/10.1193/1.1586011
Sumer, A., Kersting, R.A. and Hutchinson, D.A. (2009), “Nonlinear analysis of pre-Northridge steel high-rise building using modal-pushover-based ground motion scaling procedure”, In: *Improving the Seismic Performance of Existing Buildings and Other Structures*, pp. 103-113.
USGS Website: https://earthquake.usgs.gov/hazards/hazmaps/
Vamvatsikos, D. and Cornell, C.A. (2002), “Incremental dynamic analysis”, *Earthq. Eng. Struct. Dyn.*, **31**(3), 491-514. https://doi.org/10.1002/eqe.141
Weng, Y.T., Tsai, K.C. and Chan, Y.R. (2010), “A ground motion scaling method considering higher-mode effects and structural characteristics”, *Earthq. Spectra*, **26**(3), 841-867. https://doi.org/10.1193/1.3460374

CC